WPI

Interaction of Gold Nanoparticles with a Supported Lipid Bilayer Using Quartz Crystal Microbalance with Dissipation

Thesis submitted to the faculty of

Worcester Polytechnic Institute

In partial fulfillment of the requirements for the

Degree of Masters of Science in Chemical Engineering

25 April, 2013

By

Kellie Lynne Waterman

Terri Camesano, Ph.D., Professor, Research Advisor

Department of Chemical Engineering of Worcester Polytechnic Institute

David DiBiasio, Ph.D., Associate Professor, Department Head

Department of Chemical Engineering of Worcester Polytechnic Institute

Acknowledgements

I would like to thank the National Science Foundation for funding our research, as it would not have possible to pursue and accomplish the studies and goals proposed.

I am very grateful for the support and assistance of my Advisor, Dr. Terri Camesano who enabled me to overcome the many obstacles and setbacks we experienced along the way with this research. It would have been impossible to complete this project and thesis without her encouragement. I would like to thank my lab mates Kathleen Wang, Todd Alexander and Lindsay Lozeau for their help, support and friendship through the wonderful and demanding two years I have had the opportunity in attending WPI. Without support of Dr. Camesano and my lab mate friends I could not have accomplished so much.

I would also like to extend a special thanks to the undergraduate students, Theresa Logan, Michelle Ly, Thomas Finelli, Houssam Lazkani and Andrew Carey, who worked so hard to provide results for this research.

I would like to extend much gratitude to Dr. Geoffry Bothun, my undergraduate advisor at University of Rhode Island, for collaborating with us on this project and allowing the use of his lab and equipment in order to accomplish our goals. I would also like to thank Dr. Lambert, Dr. Duffy and Dr. Prusty Rao for allowing me the use of their equipment, which aided greatly in accomplishing our goals.

Abstract

Nanoparticle toxicity has become a major topic of interest due to the inevitable exposure of these nanomaterials to both humans and the environment. Nanotechnology is a rapidly growing industry with diverse material resources and an extensive market for commercialization and introduction of nanomaterials into consumer products. The problem with this flourishing technology is that it has far outgrown research based on the safety and toxicity of the nanomaterials, which in bulk are generally nontoxic. The need for research in determining the toxic effects on cells and the implications it may have on the environment have grown but the different techniques, cell systems and nanoparticles employed are generally to diverse and conflicting in overall results that determination toxicity is nearly impossible. The need for a universal technique to study the interaction of nanoparticles with cells and decouple the molecular effects (chemical properties) from the "nanospecific" effects (including size, concentration, surface charge, functionality and polarity) is apparent. It is additionally necessary to determine the mechanisms associated with nanoparticle-induced cytotoxicity in order to better understand the problems posed to both human and environmental health and then develop new safer nanoparticles.

Therefore, the focus of this study is to determine the nano-specific (physical) properties, including size and functionalization that cause toxicity, specifically through interaction with a cell membrane. A supported lipid bilayer (SLB) composed of L-α-phosphatidylcholine (egg PC) was used as a model cell membrane to test the effects of 2, 5, 10 and 40 nm gold nanoparticles (AuNPs). Given the imminent exposure of nanoparticles to the environment it is important to determine how nanoparticles would behave in the presence of natural organic matter or polymers which are naturally present in environmental systems. Poly(methacrylic acid) (PMA) can be used to represent the polymers normally found in the environment. AuNPs were diluted in PMA in order to simulate fundamental environmental conditions. Analysis was done using a quartz crystal microbalance with dissipation (QCM-D), which

measures the frequency (***f***) and dissipation (**D**) changes directly associated with mass and conformation changes of the SLB. Different overtones for *f* and D allow for theoretical interpretation of changes correlated to different layers of the membrane. The 2 and 5 nm particles were found to interact strongly with the lipid bilayer by adsorbing to and/or partially/completely penetrating into the lipid bilayer presumably due to a hydrophobic coating caused by PMA adsorption to the NP surface. The penetration caused a much more rigid membrane due to higher lipid packing caused by nanoparticle addition. The 10 and 40 nm particles interaction with the bilayer were not affected by the presence of PMA. Both AuNP sizes removed mass from the membrane with losses similar in de-ionized water and PMA solution. Removal of membrane mass (lipids/hydration) caused a more flexible membrane. It was determine that sized is the limiting factor for nanoparticle solubilization into the membrane. It can be concluded from the results that size coupled with natural organic matter affects the cytotoxicity of the nanoparticles to the membrane.

A study was done with 12 nm functionalized AuNPs in the presence of humic acid, a well-known and more complex and realistic model for natural organic matter. A PC lipid bilayer was used to simulate a model cell membrane and QCM-D techniques were utilized in the determination of toxicity and mechanistic interaction of nanoparticles with a lipid bilayer. Functionalized AuNPs were shown to decrease the rigidity of the lipid bilayer by increasing the dissipation and decreasing the mass associated with the adsorbed film (SLB). The presence of humic acid stabilized the nanoparticles and provided increased electrostatic repulsion which resulted in decreased mass losses from the membrane and much smaller decreases in membrane rigidity. It was concluded that presence of humic acid reduces the effects of functionalized nanoparticle interaction with a lipid bilayer. These results may mean that natural organic matter has the ability to reduce the cytotoxic effects of nanoparticles released into the environment.

Overall, the QCM-D was found to provide valuable information regarding the possible toxic properties and mechanisms in which different gold nanoparticle interact with a supported lipid bilayer under environmental conditions. The information provided by the studies performed has shed much light

on the interaction of gold nanoparticles with a supported lipid bilayer in the presence of model natural organic matter. The experiments done in this study are the first steps towards developing an assay with the ability to determine the toxic physical properties and mechanisms by which nanoparticles interact with lipid bilayers will greatly aid in development of non-toxic nano-materials. The technology and techniques used in this study will greatly improve the field by solidifying one technique to use in the quantitative approach studying nanoparticle/cell interactions. The use of AFM techniques in conjunction with the QCM-D would be highly beneficial by facilitating better understanding of the exact mechanisms by which nanoparticles induce cytotoxicity.

Authorship

The contents of this thesis are representative of the work done by the primary author. Contributions to this project were made by Theresa Logan, Michelle Ly, B.S. candidates in Chemical Engineering at Worcester Polytechnic Institute and Thomas Finelli, Houssam Lazkani and Andrew Carey, B.S. graduates in Chemical Engineering at Worcester Polytechnic Institute. As a group they participated in collecting data from experiments performed using the quartz crystal microbalance with dissipation.

Table of Contents

Table of Figures

Table of Tables

Chapter 1

The Effect of Gold Nanoparticle Size on the Interaction with a Supported Lipid Bilayer (SLB) Using Quartz Crystal Microbalance with Dissipation (QCM-D)

1.1 Abstract

The rapid growth and development of engineered nanomaterials coupled with an extensive material base has led to increasing incorporation into consumer products. Due to inevitable human and environmental exposure to a diverse array of nanomaterials, much research has been aimed at determining the toxic effects associated with these materials. The focus of this study is to determine the nano-specific (physical) properties, including size and functionalization that cause toxicity, specifically through interaction with a cell membrane. A supported lipid bilayer (SLB) composed of L-α-phosphatidylcholine (egg PC) was used as a model cell membrane to test the effects of 2, 5, 10 and 40 nm gold nanoparticles (AuNPs). Given the imminent exposure of nanoparticles to the environment it is important to determine how nanoparticles would behave in the presence of natural organic matter or polymers which are naturally present in environmental systems. Poly(methacrylic acid) (PMA) can be used to represent the polymers normally found in the environment. AuNPs were diluted in PMA in order to simulate fundamental environmental conditions. Analysis was done using a quartz crystal microbalance with dissipation (QCM-D), which measures the frequency (***f***) and dissipation (**D**) changes directly associated with mass and conformation changes of the SLB. Different overtones for *f* and D allow for theoretical interpretation of changes correlated to different layers of the membrane. AuNPs on the size order of ≤ 5 nm promoted a more rigid membrane whereas AuNPs ≥ 10 nm gave a more flexible membrane. The addition of polymer was found to increase the Δf experienced by the AuNPs ≤ 5 nm during interaction with the supported lipid bilayer. PMA was found to change the interaction mechanism of the AuNPs ≤ 5 nm, by promoting adsorption and/or partial/complete penetration into the lipid bilayer. Given these results, it was concluded that NPs have the ability to interact and possibly disrupt cell membranes. It can

be specifically stated that NP size effects the interaction with SLB and the addition of polymer influences NPs 5 nm ≤ interaction, by increasing mass addition to the adsorbed membrane. The results may aid in establishing an assay that will allow the general analysis and interpretation of the mechanisms controlling nanoparticle toxicity.

1.2 Introduction

Nanotechnology has contributed greatly to a variety of consumer products, many of which will consequently result in the introduction of nanoparticles into the environment through accidental exposure, controlled release or wastewater treatment[1,2]. Concerns over environmental exposure to nano-materials have been raised due to the lack of knowledge on the environmental chemistry, transport and ecotoxicology of the nano-materials[3]. The rapid growth and development of nanotechnology and nanoparticles has initiated important evaluations of environmental and health impacts of nano-materials[4]. The identification of the hazardous nanomaterials and the properties associated with toxicity presents a significant challenge due to the variety of nanomaterials developed and the vast array of properties associated with each material[5].

The colloidal stability of nanoparticles in aquatic environments controls the fate and transport of these particles which is critical for determining their overall environmental impacts[6]. Aggregation is known to strongly impact the cellular reactivity and toxicity of nanoparticles[7]. Natural organic matter (NOM) has the ability to modify nanoparticle properties by adsorbing to the surface of the particles and forming a coating, which has been found to enhance the stability of aqueous nanoparticle dispersion and decrease aggregation[8]. It is known that natural organic matter including humic substances significantly impact the surface properties of nanoparticles due to the increase in electrostatic repulsions[7]. Because NOM is ubiquitously found in natural environments, it would be pertinent to conduct toxicity investigations in the presence of NOM in order to determine what aggregations effects it possess for nanoparticles[4]. The full magnitude of nanoparticle toxicity in the natural environments would not be likely determined in the absence of natural organic matter[7].

Understanding the nanoparticle-cell interaction will improve awareness of potential nanoparticle toxicity, a critical prerequisite in developing nanotechnology for drug delivery and diagnostics in vivo[9]. However, there is much controversy over cytotoxicity studies with nanoparticles due to the vast array of cells used in the studies[9]. By using lipid bilayers, which are common to cellular life and mimic the cell membrane structure, it will mitigate differences in cell lines and aid in determining the mechanistic nanobio interaction and provide insight into nanotoxicity[9].

Nanoparticle interaction with cell membranes and cytotoxicity has been studied extensively with regards to the chemical property of the materials used. It has been shown in several studies that given the chemical nature of particulates were very similar, nanoparticle and microparticles were able to induce very different effects when interacting with cell membranes[10]. These results coupled with the knowledge that such interactions may not be determined by biochemical factors, have directed research to be focused on the morphology of the nanoparticles. Physicochemical factors, specifically size, surface charge density and polarity have been linked to the ability of the nanoparticles to strongly interact with cell membranes[10]. Studies have shown that strong membrane interaction resulted in either adsorption to the membrane or compromised the membrane integrity resulting in the formation of holes[10]. The resulting morphology was therefore dependent on the size and surface charge of the nanoparticle rather than the biochemical properties of the material. It can be concluded that the mechanism of cell membrane disruption was therefore, a consequence of purely physical characteristics of the nanoparticles.

Figure 1 provides a schematic description of the various modes of nanoparticle membrane interaction and the mechanisms by which lipid membrane disruption may occur. Nanoparticles are thought to have the ability to adsorb to the surface, partially or completely solubilize into the hydrophobic interior of the lipid chains (Figure 1A). As a consequence of these types of nanoparticle interactions with the membrane, the molecular packing of the bilayer becomes disrupted. The lipid chains respond to this disruption by stretching in order to maintain the molecular space filing requirement of the lipid bilayer and eliminate voids. Membrane thinning and chain stretching are energetically unfavorable processes, which at a critical nanoparticle dosage, may result in the formation of cylindrical pores (Figure 1B,C).

Two types of pores may be possible including one seen in Figure 1B where the pore walls are lined with the nanoparticles or in Figure 1C, where a toroidal pore has formed in which both lipids and nanoparticles make up the pore wall. Under certain conditions of increased strain on the membrane due to nanoparticle interaction, membrane lysis may occur leading to the formation of lipid/nanoparticle aggregates (Figure 1D). At the critical nanoparticle dosage where the membrane may experience physical changes, we can conclude that the structural integrity of the membrane has been compromised.

Although many studies have been published regarding the toxicity of nanoparticles to cell, the nature of cytotoxicity associated with the "nano-specific" (physical) properties of the nanoparticle and the mechanisms by which toxicity occrurs is still not well understood. Therefore, the goal of this research was to provide a fundamental way in which to quantify size related nanoparticle toxicity under sterile lab and environmental conditions. The purpose was to be able to determine if mechanistic interactions were modified and cytotoxicity was quantitatively altered by the presence of natural organic matter. In this study poly(methacrylic acid) (PMA) was used in order to simulate the conditions found in the environment. Due to their increasing application in diagnostics and drug delivery as well as the nontoxic properties of the bulk metal, gold nanoparticles were chosen as the model nanoparticle for this study.

1.3 Materials

Spherical gold nanoparticles (AuNP) were purchased from NANOCS (New York, NY) in the diameters of 2, 5, 10 and 40 nm with a narrow size distribution of <15% according to the manufacturer. Zeta potentials were measured at the University of Rhode Island using a Nano Series Zetasizer (Malvern, Worcestershire, UK) with folded capillary cells revealed average measurements of -48.8, -46.7 and -56.8 for the aforementioned AuNP sizes, respectively. The original stock NP solutions were stored in de-ionized water with small amounts of sodium citrate and tannic acid at 7 °C in a light impenetrable container. The concentrated AuNP solutions (2, 5, 10 and 40 nm) were diluted with de-ionized water or poly(methacrylic) acid solution to a concentration of $7.14x10^{10}$ particles/mL.

Poly(methacrylic acid) was purchased from Polymer Source, Inc. (Quebec, Canada). The polymer solution was prepared by adding 0.20 g of poly(methacrylic acid) powder to 200 mL of de-ionized water and sonicated for 30 min in a water bath ultrasonic cleaner (Bransonic, Danbury, CT) to yield a concentration of 0.001 g/mL, and stored at 7 °C.

L-α-phosphatidylcholine (egg, chicken) (PC) with purity > 99% was purchased from Avanti polar lipids. 1 g of egg PC powder was solubilized in 10 mL of ethanol to yield a 100 mg/mL solution stored at -20 °C. Other chemicals were purchased from Sigma-Aldritch (St. Louis, MO).

A buffer solution made of 10 nM Tris (hydrozymethyl) aminomethane with ≥ 99.9% purity and 100 nM sodium chloride, +80 mesh particle size, pH 7.8, was prepared in de-ionized water.

QCM-D sensor crystals (5 Hz), reactively sputter-coated with silicon dioxide, were purchased from Biolin Scientific (Gothenburg, Sweden). Crystals were cleaned using modified Q-sense protocols which include an ethanol rinse followed by de-ionized water then 2% sodium dodecyl sulfate rinse. The crystals are then rinsed in de-ionized water again and dried with nitrogen gas. To remove any other organic contaminants and slightly oxidize the sensor surface, the crystals undergo two cycles of 45 s oxygen plasma cleaning using Plasma Prep II (SPI Supplies, West Chester, PA). Under favorable conditions the sensor crystals can be used up to 10 times.

1.4. Methods

1.4.1 SLB Formation

An egg PC vesicle solution was prepared according to published procedures by Barenholz et al and Keller et al. 0.15 mL of the 100 mg/mL egg PC solution was dried with nitrogen gas, desiccated for 24 h and rehydrated with 6 mL of Tris-NaCl buffer solution[11,12]. The lipids were re-suspended by vortexing for 15 s on a mini vortexer (Fisher Scientific Inc., Pittsburgh, PA) and underwent 5 cycles of freeze-thaw-vortex 15 s. Small unilamellar lipid vesicles (SUVs) were formed by sonication of the egg PC solution in a glass tube with a ultrasonic dismembrator (Model 150T, Fisher Scientific, Waltham, MA) for 30 min in pulse mode with a 30% duty cycle (3-second pulse at an amplitude of 60,

followed by a 7-second pause) immersed in an ice bath[11,12]. Probe particles were removed from the solution through centrifugation (Eppendorf Centrifuge 5415 D) at 16000 g's for 10 min at 23 °C. The supernatant was decanted from the pellet and stored under nitrogen gas at 7 °C for up to a month. It is recorded that the solution was viable for up to 6 months[12]. However, after one month's time it was found that bilayer formation no longer occurred. Before use, lipid vesicle suspensions were diluted to 0.1 mg/mL if not otherwise stated. All stock and dilute solutions were vortexed for 15 s prior to use.

1.4.2 Quartz crystal microbalance with dissipation monitoring (QCM-D)

QCM-D measurements were performed with the Q-sense E4 system (Biolin Scientific, Sweden). Quartz sensor crystals coated with silicon dioxide were placed in four flow modules and exposed to different solutions continuously delivered to the measurement chamber (flow rate of 0.15 mL/min unless otherwise stated) by the aid of a peristaltic pump (IPC high precision multichannel dispenser, ISMATEC, Switzerland).

The piezoelectric properties of the sensor allow the measurement of the interaction of (soft) matter with the surface of the senor related to attached mass (including coupled water) or change in resonance frequency, f, and the dissipation, D, related to frictional (viscous) losses in the adlayer. Changes in the dissipation and normalized frequency ($\Delta f_{norm} = \Delta f_n/n$, with n being the overtone number) of the third, fifth, seventh, ninth and eleventh overtone ($n = 3, i.e., 15MHz$) are presented. The Suaerbrey equation for rigid films determines the inverse relationship between mass adsorption and frequency change, with mass sensitivity constant $C = 17.7\ ng \cdot cm^{-2} \cdot Hz^{-1}$ for 5 MHz sensor crystals,

$$\Delta m = -\frac{C \cdot \Delta f}{n}$$

where an increase in mass is directly proportional to a decrease in frequency. Energy dissipation changes are associated with the rigidity of the adsorbed film. The normal mass and dissipation sensitivities of QCM-D measurements in liquid are ~1.8 ng/cm^2 and ~0.1 x 10^{-6}, respectively.

The third through eleventh harmonics of the sensor crystal's natural frequency (5 MHz) were measured and normalized automatically to each overtone (f/n, where f is frequency and n is the harmonic number) by the Q-Sense software. The fundamental frequency was not analyzed due to its highly sensitive nature to changes in the bulk solution during flow[13].

1.4.3 AuNP/H_2O control solution interaction with SLB

QCM-D sensors were cleaned according to adapted manufacturer protocols (supplementary information). Sensor harmonics, frequency and dissipation, were calibrated in air and stabilized in Tris-NaCl buffer delivered to the measurement chamber at a continuous rate (flow speed 0.15 mL/min) by the aid of a peristaltic pump (IPC high precision multichannel dispenser, ISMATEC, Switzerland) for 10 min. All solutions were delivered to the chamber using the same flow speed. The SUV solution was allowed to flow over the sensor crystals for 6 min to form a stable SLB. The sensors with formed SLB were rinsed in buffer for 8 min to remove excess un-ruptured vesicles. A baseline for the SLB in de-ionized water was then established for 8 min and the AuNP solution was washed over the membrane for 10 min. The SLB was then rinsed in de-ionize water and Tris-NaCl buffer for 8 min each, respectively. Each experiment was repeated 3 times for a total of 12 replicates for each size of NP.

1.4.4 AuNP/polymer sample solution interaction with SLB

The preceding procedure was followed with the addition of rinsing the membrane in a polymer solution for 8 min before and after the introduction of AuNPs into the chamber. The AuNP solution used in this section was diluted to $7.14x10^{10}$ particles/mL with 0.001 g/mL polymer solution before being introduced into the module chamber. All other aspects of the procedure remained the same including replicate data collected.

1.4.5 Data Analysis

Nanoparticle toxicity was determined by using data compiled from plots and data sets obtained from the QCM-D. Two different experiments were performed; 1) different sized gold nanoparticles diluted in water, 2) different sized gold nanoparticles diluted in a PMA solution. The raw data from the QCM-D was represented in plots which showed ~ 20 min time different between the time when AuNP/water solution was added and the time when AuNP/PMA solution was introduced. The difference in time can be directly attributed to the necessity of stabilizing the system to the viscosity of the nanoparticle solution that is introduced (i.e. de-ionized water or PMA solution).

Data for the Δf for each of the six overtones (3, 5, 7, 9 and 11) was compiled and averaged according to the number of replicates performed for each AuNP size. Frequency changes were recorded at the times one min before changing over to AuNP solution and one min before changing into buffer solution from de-ionized water. Standard deviation values were taken from the frequency change data and used to produce bar charts highlighting the difference in frequency change between each overtone, which provides information on how the AuNPs interact with each layer of the chamber/membrane.

Plots of D/f vs. functionalized AuNP were made in order to observe the change in viscoelastic properties per mass change for each type of functionalized AuNP. Averaged values for D and f were taken at one minute before AuNP solution introduction into the chamber (i.e. changing from PMA into NP/PMA solution) and one minute before de-ionized water rinse (i.e. changing from PMA into de-ionized water). The D and f plots should provide insight on viscosity changes of the SLB associated with AuNP interactions with the supported lipid bilayer.

1.5 Results

1.5.1 Raw QCM-D Data Plots

The raw data, expressed in plot form, for an experiment performed with AuNPs diluted in de-ionized water with the QCM-D is presented in Figure 1.2. The formation of the bilayer was monitored by observing the changes associated with frequency and dissipation corresponding to the blue and red lines, respectively. Bilayer formation corresponds to the large changes in frequency and dissipation within the first 6 min of the experiment. The membrane was then stabilized in Tris-NaCl buffer, depicted in the horizontal slope of both D and f from 8 to about 15 min. The introduction of de-ionized water after flowing buffer is depicted by the small increase in frequency accompanied by the large decrease in dissipation, which is followed by NP and de-ionized water solution. At ~42 min, an appreciable drop in frequency and significant increase in dissipation was observed, as a result of the re-introduction of Tris-NaCl buffer.

Figure 1.3 shows a typical QCM-D plot for the interaction of AuNPs, in the presence of PMA, with the supported lipid bilayer. This plot was similar to Figure 1.2, although, 16 min are added to the overall experimental procedure due to the introduction of the PMA solution before and after the introduction of the NP/PMA solution. Nanoparticle interactions are not obvious at this scale, but small changes in the dissipation and frequency are occurring.

1.5.2 Effect of Nanoparticle size on Membrane Interaction

Experiments were performed with each of AuNP diluted in de-onized water in order to directly compare and determine how the addition of polymer will impact the interaction of nanoparticles with a lipid bilayer. The 2 nm AuNPs displayed a lack of interaction with the model membrane and the large error associated with each overtone can be attributed to noise due to no interaction (Figure 1.4A). The AuNPs larger than 2 nm each had a positive change in frequency corresponding to a decrease in mass, when interacting with the SLB. The 5 nm AuNPs had the most consistent change in mass, with positive

increases in frequency across the range of overtones and losses in mass spanning the width of the membrane (Figure 1.4B). In Figure 1.4, C and D, the 10 and 40 nm AuNPs appear to have very similar interactions with the bilayer. The 40nm AuNPs have an overall smaller interaction with a reduction in mass loss, particularly with the 9^{th} overtone. The 10 nm AuNPs has a similar trend followed by the 5 nm nanoparticles, with a consistent decrease in mass seen across the width of membrane. A reduction in mass can be seen however, in the 11^{th} overtone for the 10 nm AuNPs (Figure 1.4C).

1.5.3 Effect of Poly(methacrylic acid) on Nanoparticle/Membrane Interaction

The 2 nm AuNPs in Figure 1.4E have a significant decrease in frequency across all overtones indicating that the addition of polymer has a substantial impact on the interaction between the AuNPs and the SLB. There was a large mass increase associated with the regions closets to the crystal surface (overtones 7, 9 and 11) for the 2 nm AuNPs. The overtone vs. frequency data for the 5 nm AuNPs (Figure 1.4F) was unique because of the significant negative change in frequency achieved with the addition of polymer. There was a nearly uniform mass addition across the width of the membrane for the 5 nm AuNPs. It would seem that the polymer did not alter the interaction of the 10 nm AuNP with the bilayer in comparison with the control (Figure 1.4G). Figure 1.4H shows that the 40 nm AuNPs did experience a change in the interaction with the SLB with the addition of the polymer. Mass was most significantly lost at the surface, where the membrane is in contact with solution. There is very little mass loss near the sensor surface.

1.5.4 Zeta Potential Results

Zeta potentials were measured in Dr. Geoffry Bothun's lab at The University of Rhode Island. A compilation of the zeta potentials can be seen in Table 1.1. Data was not collected for the 40 nm size nanoparticles, however zeta potential data (not shown) measured for a 80 nm bare gold particle from the same manufacturer was obtained and given the results (-45.7 mV) it can be concluded that the 40 nm

AuNP zeta potential would be similar to the 10 and 80 nm particles. All the nanoparticles were found to be significantly negative and fairly similar in value despite the range in size.

1.5.5 Comparing Dissipation to Frequency with Respect to Nanoparticle Size

In order to determine the effect of nanoparticle size on the conformation of the supported lipid bilayer dissipation and frequency were compared for the four nanoparticle sizes (2, 5, 10 and 40 nm) diluted in de-ionized water. Figure 1.5 depicts the change in dissipation versus the change in frequency. The 2 nm AuNP diluted in de-ionized water had a linear and nearly horizontal slope. The data points appear to be very closely packed illustrating little to no change in dissipation for very small changes in frequency. Figure 1.5C shows the 5 nm AuNP diluted in water D/*f* plot. The slope of the data seems to be positive given increasing dissipation with increasing frequency. Again, the data points were very tightly packed together. The data for 10 nm AuNPs diluted in water have an unclear trend as the data was very scattered. The 40 nm AuNPs diluted in water had the clearest trend with very distinct negatively sloping linear data. However, it can be seen the data appears to split into two different data sets with a large gap seen between ~1 Hz to ~22 Hz for frequency. The two data sets have very closely packed data points representing small changes in dissipation and frequency.

1.5.6 The Comparison of D/*f* for AuNPs Diluted in PMA

Dissipation and frequency values were measured using the QCM-D for 2, 5, 10 and 40 nm AuNPs diluted in the PMA solution. The dissipation and frequency values for each nanoparticle size were compared in order to determine the effects of nanoparticle interaction with the supported lipid bilayer in the presence of PMA. The plots in Figure 1.5 illustrate the D/*f* for the four nanoparticle sizes. The 2 nm AuNP/PMA had the most unique plot with two different sloping regions labeled as 1 and 2. The first region had a much steeper slope, which in the second region become much more gradual. Both slopes were negative. The 5, 10 and 40 nm AuNPs diluted in PMA had very similar trends in terms of being linear. The 5 nm appears to have a positive slope; with much more tightly packed data points near the

larger values of dissipation and frequency and slightly spread out data points for the lower values of D and *f*. The plot for the 10 nm AuNPs had a nearly horizontal plot with very closely packed data points. The 40 nm AuNPs may have a slightly negative slope although it was difficult to determine due to the widely scatter nature of the data points.

1.5.7 Comparison of Membrane Viscoelastic Changes to Nanoparticle Size

The comparison of D/*f* with respect to size in the presence of PMA was done in order to compare how different sizes affected the conformation of the supported lipid bilayer when in the presence of PMA. The 2 nm AuNP had a significantly large negative value of D/*f* in comparison to the other size nanoparticles (Figure 1.6). The 5 nm AuNP was negative, although had a slightly smaller value than that seen for the 2 nm. The 10 and 40 nm AuNP diluted in PMA had positive values of D/*f*. The 10 nm had a substantially larger positive value (0.02) than the 40 nm nanoparticles (0.007).

1.6 Discussion

1.6.2 Application of Membrane Destabilization Theory

The plots in Figure 1.4 offer much insight into how the AuNPs were interacting with the SLB by providing information related to mass changes across the different layers of the membrane. Use of the QCM-D allows theoretical interpretation of how and where mass addition is occurring in relation to the crystal surface. Changes in frequency with regards to overtones 11 and 9 provide insight on the layers of the SLB in contact with the water layer trapped under the membrane, whereas overtones 3 and 5 are associated with fluid flow in the chamber and the surface of the membrane, respectively. Looking at mass addition specifically, the 2 nm AuNPs diluted in PMA have a large negative Δf that occurs in the higher overtones. This may indicate that the nanoparticles are able to be solubilized into the hydrophobic SLB interior through two mechanisms: 1) penetrating through the membrane or 2) forming pores stabilized by nanoparticle or a combination of the two. The 5 nm AuNPs diluted in PMA also have significant increases negative Δf which indicate that this size of nanoparticle may also be capable of interaction with

the SLB through the two above mentioned mechanisms. However, for the 5 nm AuNPs diluted in PMA, there was an equal decrease in frequency seen for each overtone which may indicate pore formation where nanoparticles line the pore walls. It may also indicate that 5 nm AuNPs in the presence of PMA were able to insert in a uniform mechanism across the width of the membrane. It can be concluded that the results for the 2 and 5 nm AuNPs in PMA help to support the destabilization membrane theory proposed in this study, although it was unclear which specific mechanism of the theory can be attributed to the addition of mass.

The large increases mass seen for the 2 and 5 nm AuNPs diluted in PMA were largely associated with the region closest the membrane surface, meaning that the nanoparticles were able to, using one of the mechanisms proposed, penetrate through the membrane. The affinity of the nanoparticles for the interior of the membrane may be in part due to the addition of the PMA to the solution. The presence of PMA may have the ability to alter the polarity of the molecules, making them hydrophobic and act as a driving forced for concentration in the interior of the membrane. Natural organic matter (NOM), also known as polymers, has been found to alter the properties of nanoparticles by absorbing onto the surface of the nanoparticles[14]. The substitution and/or covering of the original stabilizers found on the surface of the nanoparticles have been found to affect the surface charge and chemistry of the nanoparticles[14]. In a study done by Nason et al, the adsorption of NOM onto the surface of the engineered nanoparticles was found to influence the surface chemistry, biding affinity and colloidal stability similarly to the capping agent generally found on nanoparticle surface[14]. Therefore, PMA, which represents typical polymers found in the environment, may have similar effects on the nanoparticles of this study, altering their surface chemistry and charge to that of a hydrophobic particle and thus providing the driving force for membrane penetration. Gold, which is generally hydrophilic when clean, has the tendency to become easily coated with organic materials, modifying the polarity to hydrophobic. It was probable that the mass addition may have been a result of either a single mechanism or a combination of mechanisms (pore formation, adsorption or penetration). Although it is unclear which specific mechanism dominates the addition of mass, the inconsistent addition of mass across the width of the bilayer would suggest

solubilization was most likely. Inconsistency in mass addition would generally rule out the pore formation model.

The data presented in Figure 1.4 may suggest that losses in mass have a direct correlation to both PMA addition and nanoparticles size. According to the size of the particles, it can be determined that the larger sizes of AuNPs (≥ 10 nm), diluted in either de-ionized water or PMA solution, interact with the model membrane surface and possibly have the ability to remove mass. The 10 and 40 nm AuNPs diluted in de-ionized water (Figure 1.4G, H) have very similar reduction in mass patterns, which indicate that mass and possibly hydration has been removed from the membrane. Although mass losses extend into the interior of the membrane, the irregularity of the Δf make it unlikely that nanoparticles are able to remove lipids close to the sensor surface. The mass losses could be attributed to rearrangement of lipid groups filling membrane gaps due to lipid losses experienced at the surface of the membrane. Possible hydration losses from the water layer located between the sensor surface and membrane from gaps created in the membrane may have contributed to positive changes in Δf. The 40 nm AuNPs diluted in PMA suggest that mass losses were directly related to membrane and/or hydration removal from the surface of the membrane. The 5 nm AuNP diluted in de-ionized water experienced mass losses at every overtone, with near uniformity, meaning that possible pore formation may have occurred coupled with hydration losses from the interior water layer. Lipid may have been removed in the process of pore formation and the combined mass loss overcomes the addition of nanoparticles in the pores. AuNPs ≥ 5 nm interacted and removed mass from the membrane. The 5 nm AuNPs were able to remove larger quantities of mass from the interior of the membrane than the 10 and 40 nm AuNPs which had overall smaller mass changes. There was a size threshold for mass loss/addition in the region between 5 and 10nm. This observation was also true for AuNPs interacting with the membrane interaction in the presence of polymer, where decreases in Δf coincide with increasing NP size as seen in Figure 1.4E and F.

1.6.3 Interaction in the Presence of PMA

The addition of poly(methacrylic acid) to the NP solution had varying result for the different sizes of NP and there appears to be a trend associated with NP size. According to the results seen in Figure 1.4, the addition of the PMA caused the nanoparticles ≤ 5 nm to interact in a way with the SLB that resulted in mass addition. The controls for both 2 nm and 5 nm AuNPs demonstrated that nanoparticle interaction, insertion or adsorption to the membrane caused negative Δf values. Given that the nanoparticles are hydrophilic, it can be assumed that the bare nanoparticles would be inclined to interact with the zwitterionic surface of the membrane due to electrostatic and van der Waals interactions[15,16]. This kind of interaction was depicted by the control experiments, where nanoparticles were diluted in di-ionized water (Figure 1.4E-H). The bare nanoparticles removed mass from the SLB surface, possibly due to shearing, of AuNPs electrostatically interacting or through van der Waals interactions with the polar lipid headgroups, by fluid velocity and/or hydration removal through polar interactions[15,16]. The bare gold nanoparticles are known to be negatively charged through zeta potential measurements taken using a Malvern Zetasizer (folded capillary cell, Nano Series ZS, Malvern Instruments Ltd, Worcestershire, UK) in the Bothun Lab, at the University of Rhode Island (Table 1.1). The AuNPs had similar zeta potentials (-50.7mV±5.05mV). Due to the uniform charge of the nanoparticle solutions, the particles were unable to agglomerate or aggregate in solution due to repulsive forces[16].

The AuNPs ≤ 5 nm, in the presence of PMA have added mass to the membrane through adsorption, partial or full penetration into the SLB. The 2 nm NPs appear to have a greater ability to add mass in comparison to the 5nm particles (Figure 1.4A, B). This could be in part due to the PMA coating the nanoparticles, which caused the particles to become hydrophobic and have an affinity for the interior of the membrane. Bothun has shown that hydrophobic 5.7 nm Ag nanoparticles have the ability to become internalized in the hydrophobic lipid interior of a liposome[15]. The nanoparticle diameter was near or exceeding the bilayer thickness, but due to the hydrophobic properties of the Ag decanethiol NPs, the particles were driven to insert into the hydrophobic region of the bilayer[15]. Similarly, Park et al. was able

to solubilize 3-4 nm gold nanoparticles into liposomes by coating the particles with a hydrophobic dispersing agent, stearylamine[41]. With a hydrophobic surface, the gold nanoparticles had a higher affinity for the carbon chains on the interior of the liposome[17]. The PMA may be acting in the same context, coating the particles and causing them to become hydrophobic.

AuNPs $\leq$ 10 nm are stabilized with tri-sodium citrate and small amounts of tannic acid. The tannic acid with its large molecular structure would have a much smaller coating density on the 2 nm NPs in comparison to the 10 nm NP due to the overall structure. The ratio of tri-sodium citrate to tannic acid would be much higher for the 2 and 5 nm NPs than the 10 and 40 nm AuNPs. Due to the larger amounts of tri-sodium citrate, the smaller nanoparticles are more likely to have a smaller overall diameter, which would aid insertion into the membrane. The interaction of the PMA with the tri-sodium citrate and small amounts of tannic acid would result in hydrophobic molecules as a result of the carboxylic acid group on the PMA removing the Na^+ ion from the tri-sodium citrate and a H_2O from the carboxyl group on the PMA to form an ester bond. The configuration of the ester bond results in the polar group being trapped nearest the nanoparticle surface and the nonpolar region of the PMA exposed to the surrounding solution creating a hydrophobic particle. Given that the PMA used was a 79 monomer long molecule, it reacted with both the tannic acid and tri-sodium citrate molecules and wraps the AuNPs in a hydrophobic coating. The PMA was a long chain molecule and it has been previously determined that NP size directly correlates with the ability of the nanoparticle to insert into a lipid bilayer[15,17]. Therefore, as the NP size increases, a threshold is reached in which the size overtakes the hydrophobicity of the nanoparticle and the large nanoparticles are not able to insert into the membrane. The 2 nm has the largest increase in mass and ability to insert into the SLB and the 5 nm AuNPs, while it was still able to penetrate the bilayer, the interaction was reduced by half as a result of NP size and possibly the overall diameter induced by PMA coating. The large AuNPs (10 and 40 nm) have a much larger ratio of tannic acid to tri-sodium citrate because of increased surface area, which allows for large amounts of PMA to interact and form a coating. The PMA coating greatly increased the overall diameter of larger particles, which have larger diameters

than the thickness of the membrane, overcoming the hydrophobic property induced by the PMA and preventing membrane insertion.

1.6.4 Membrane Conformational Changes in Relation to D vs. *f*

The QCM-D was able to give information regarding the changes in mass and rigidity of the membrane given the time frame of nanoparticle introduction in the presence of PMA. Comparing the change in dissipation versus frequency for the time that nanoparticles in the PMA solution were in contact with the membrane depicts the induced energy dissipated per coupled unit of mass. By eliminating time it was possible to directly relate the ratio of dissipation to frequency[18]. The comparison demonstrates how the interaction of the nanoparticles with the membrane influences the viscoelastic dampening of the crystal resonance which infers the changes in the viscoelastic properties of the adsorbed layer[19]. For example, a large D/*f* value signals a soft dissipative film, whereas a small D/*f* value indicates mass addition without significant changes in the dissipation which would signify a rigid film was formed[18,19]. Consequently, a higher value of D/*f* corresponds with a lower density adsorbed film on the sensor surface, which may be related to a more loosely packed and possibly hydrated film[20]. Given that there was a unique response per each size of nanoparticle, this type of plot could serve as a fingerprint for the particular AuNP interaction with the membrane[21].

Nanoparticles ≤ 5 nm appear to have very different mechanisms of interaction with the SLB in comparison with AuNPs ≥ 5 nm diluted in de-ionized water or PMA solution. The 2 nm AuNPs in PMA (Figure 1.5B) have a unique response with a drastic change in slope, indicating there may be two different mechanisms of adsorption. Both slopes were linear meaning a natural gradient with time. The initial slope was much steeper, indicating a rapid change in the conformation of the membrane. The negative slope for both regions of the 2 nm AuNP/PMA plot indicated a decrease in dissipation with an increase in frequency, which directly correlates to an increase in rigidity of the membrane. The steep portion of the plot may indicate that the interaction of the nanoparticles happens instantaneously and possibly saturates the membrane. In the second region of the graph, where the slope was very gradual, meaning only small

changes in the rigidity of the membrane were taking place given that very few nanoparticles were able to interact after the initial saturation. This type of two phase interaction was seen by Frost et al. with insulin-loaded nanoparticles in contact with a model cell membrane formed from POPC and POPS lipids. The two phases were attributed to NPs adsorbing to the bare lipid membrane in the first phase and in the second phase NPs were adsorbing to a surface partially or fully covered by NPs[22]. Several other groups have reported similar trends associated with conformational changes in the adsorbed medium (Feiler et al.[19], Hook et al.[18]) suggesting that it was possible for the 2 nm AuNPs to have a two phase interaction.

The 5 nm AuNPs in the presence of PMA appear to have a preliminary conformational change in the membrane caused by interactions between the SLB and NPs. Figure 1.5G initially has a small slope indicating an increase in the D/*f* ratio, which corresponds to a slightly more flexible membrane (increasing D). The interaction then levels off and appears to be constant which signifies that the viscoelastic properties of the membrane do not change significantly after initial contact with the nanoparticles. From the previous plot (Figure 1.5F) it was concluded that the 5 nm particles in PMA had a small mass addition to the SLB due to the diameter of the NPs meeting/exceeding the overall width of the membrane. The conclusions drawn from Figure 1.4F coincide well with the D/*f* plot for the 5 nm AuNPs due to the small mass addition associated with the size of the NP, resulting in small viscoelastic changes. It can be expected that the D/*f* value would initially increase due to rearrangement of the bilayer corresponding to mass addition and then become constant, which is consistent with the saturation of the membrane with NPs. Once the membrane is saturated with larger diameter NPs during primary contact, it would be less likely for any more mass to be added, resulting in a constant membrane conformation.

The 10 nm and 40 nm AuNPs have similar trends when comparing dissipation to frequency over the period of nanoparticle PMA addition. The two plots (Figure 1.5D, E) appear to follow a somewhat linear trend with a slight sloping in the negative direction. The scattered formation of the data points may be directly correlated to the mass changes see in Figure 1.4, which result in conformational changes in the membrane as lipid molecules are rearranged in order to eliminate gaps. It has been shown that the addition of hydrophobic nanoparticles instigates changes in the lipid packing and phase behavior of the

lipid bilayer[15,23]. If the PMA coating alters the polarity of the nanoparticles, thereby creating a hydrophobic particle that can penetrate the lipid bilayer, than changes seen in the plot of D/*f* correlate to conformational changes caused by nanoparticle addition to the bilayer. Although the amount of mass lost in comparison to other literature (Frost et al.[22], Feiler et al.[19], Hook et al.[18]) was very small, it can still account for the slight negative changes in D/*f*, which relate to the structure of the membrane where the film became slightly softer as mass decreased. The less tightly the packed the structure adsorbed to the crystal surface, the smaller the dissipation. The small changes in mass and viscoelastic properties of the lipid bilayer across the range of sizes of the AuNPs in the presence of PMA or the control experiment may be correlated to the generally non-toxic characteristics of gold. The concentrations used in the study (~10 µg/ mL) were significantly higher than the toxicity levels seen in other studies, which were using similar sized AuNPs with a concentration on the order of 0.6-0.75 µg/ mL[22,24].

1.6.5 Nanoparticle Size and Film Structure Correlation

The nanoparticle size was compared to the viscoelastic properties of the supported lipid bilayer in order to determine how size affected these properties. While the other plots are able to give a sense of the mass changes and how those mass changes influenced the structure of the membrane, the results did not directly compare the viscoelastic changes associated with mass change for each of the nanoparticle sizes. Figure 1.6 provides a concise plot of the D/*f* versus the size of the nanoparticles so direct comparisons may be made. The AuNPs $\leq$ 10 nm support the information previously seen in Figures 1.4 and 1.5. It would be expected for the frequency term to dominate the ratio of D/*f* for both the 2 and 5 nm particles. The smaller nanoparticles were able to penetrate into the interior of the membrane and given their small size, no appreciable conformational changes in the membrane would occur. In particular, the 2 nm AuNPs were significantly smaller than the bilayer's width, meaning the bilayer would have been much more able to accommodate the particles inclusion into the hydrophobic interior. The 5 nm nanoparticles were shown to have a smaller mass addition to the SLB, which would consequently result in a slightly higher D/*f* value which was seen in Figure 1.5. A PC lipid bilayer is known to about 5 nm in width and Bothun's

studies have shown that lipid bilayers have the ability to contort slightly with small changes to the structural conformation to allow for NPs of similar diameter to solubilize into the interior of the membrane[15,25]. It can be concluded that the 5 nm AuNPs used in these experiments, which are 0.7 nm smaller than in the previous study, would be able to insert into the hydrophobic region of the membrane with very small changes to the viscoelastic properties of the bilayer.

The larger nanoparticles are known to remove mass from the SLB, resulting in a much larger dissipation term for the ratio of D/*f*. Removal of mass from the membrane causes large structural changes as the bilayer rearranges lipids to compensate for voids or holes formed. It is evident that the significant mass losses for the 10 nm AuNPs caused a large increase in the dissipation and a much softer film (Figure 1.5). Given the large D/*f* value seen for the 10nm NPs, it would be assumed that the 40 nm particles would result in a larger value given the size of the NP had increased 4 fold. The difference in the hypothesized outcome to the one seen in Figure 1.5 could be attributed to losses in mass occurring only on the surface of the membrane whereas the 10 nm NPs causes mass loss across the width of the membrane. It may be that the bilayer only has to make minor changes in its structure to compensate for the loss from the 40 nm particles, which was why the D/*f* value is much smaller. There may be a threshold associated with the size range between the 10 and 40 nm particles and looking at data in this range would reveal where it takes place.

1.7 Conclusions

The novel approach of using the quartz crystal microbalance with dissipation to test nanoparticle toxicity on a supported lipid bilayer when in the presence of natural organic matter was successful in characterizing the mechanisms by which nanoparticles may be toxic. It was possible to further address the issue of which physical characteristics cause the nanoparticles to be toxic and how the mechanisms or toxicity changes in the presence of organic matter. The results presented in this study showed that the toxic effects of AuNPs may be directly associated to the size of nanoparticle and the environment conditions under which the particle has come into contact with a membrane. The 2 and 5 nm AuNPs in

the presence of PMA caused a negative increase in frequency indicative of an increase in mass. This may be attributed to adsorption, partial or complete penetration into the hydrophobic interior of the membrane facilitated by the hydrophobic coating of PMA as it reacts with the stabilizing groups on the nanoparticle surface. These sizes of nanoparticles consequently caused a more rigid membrane through insertion which caused tighter packing of the lipids. The NPs ≤ 5 nm removed mass or did not interact with the membrane indicating that PMA facilitated the mass addition. The larger nanoparticles (≥ 10 nm) did not experience any significant changes associated with the addition of PMA to the solution. There was a general trend of mass loss, which could be attributed to lipid or hydration removal by the nanoparticles. This generally produced a much more flexible membrane seen in the large D/*f* versus size for the larger particles which correlates with masses lost from the membrane. As the lipid layer become more loosely packed the dissipation increasing, meaning a more fluid membrane. It can be concluded from the results that both size and environmental conditions affect the cytotoxicity of the nanoparticles to the membrane.

This is the first step towards developing an assay that has the ability to determine the mechanism of nanoparticle-induced cytotoxicity by decoupling molecular effects from "nano-specific" effects. Other techniques employed have been inadequate because of their inability to separate the role of membrane destabilization from other types of cytotoxic effects. This technology will move the field forward by using a quantitative approach to study nanoparticle/cell interactions and have the capability of application in numerous nanoparticle/cell membrane combinations. It would be highly beneficial to combine these techniques with the use of the AFM in order to accurately determine the exact cytotoxic mechanisms employed by the nanoparticles.

Table 2.1 Zeta Potential Measurements for Bare Gold Nanoparticles in Water

Gold Nanoparticle Size	Zeta Potential
(nm)	(mV)
2	-48.8
5	-46.7
10	-56.8
40	N/A
80	-45.7

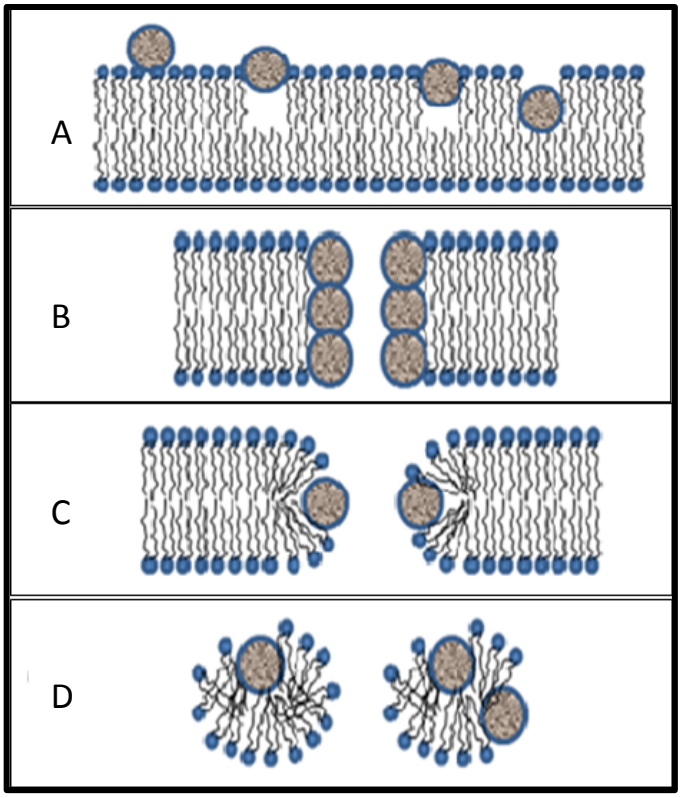

Figure 1.1 Schematic description of nanoparticle interactions with a lipid bilayer.

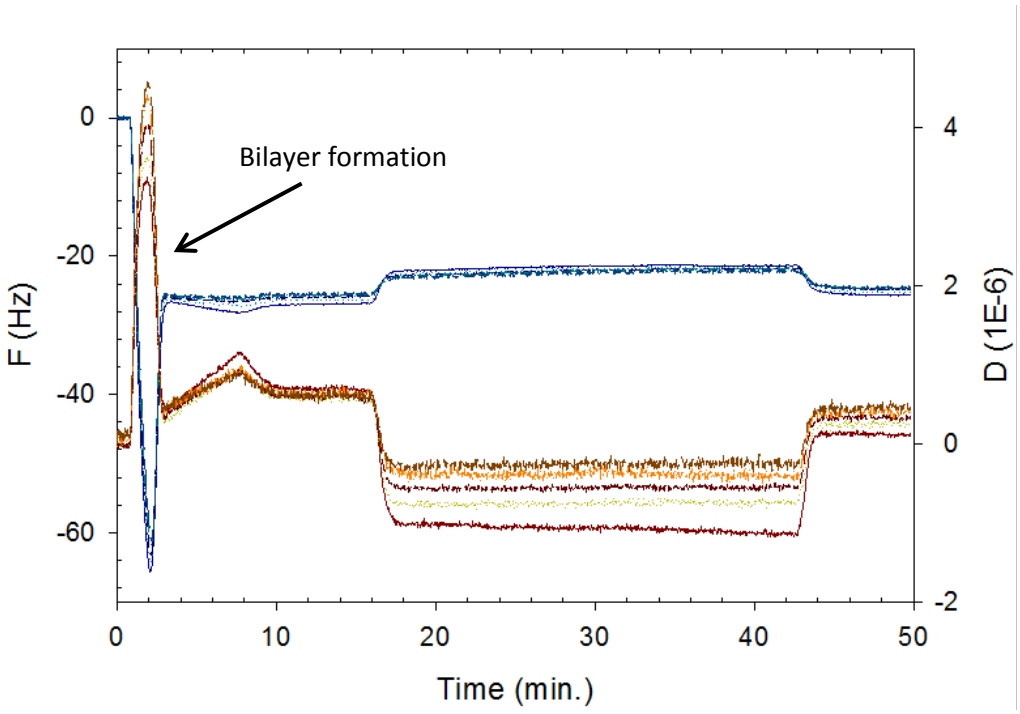

Figure 1.2 Formation of a PC bilayer on SiO_2 crystal. After the bilayer formation, buffer flows through the module to remove un-ruptured or excess vesicles. Water is then introduced to form a viscosity baseline for AuNPs introduced, followed by another water rinse. Bilayer is rinsed by buffer to complete the experiment. Blue lines represent the frequency for each overtone and red lines represent the dissipation for each overtone. Overtones 3, 5, 7, 9 and 11 are shown on the plot. (buffer rinse 6:47; water rinse 15:09; NP 23:27; water rinse 33:42; buffer rinse 41:56)

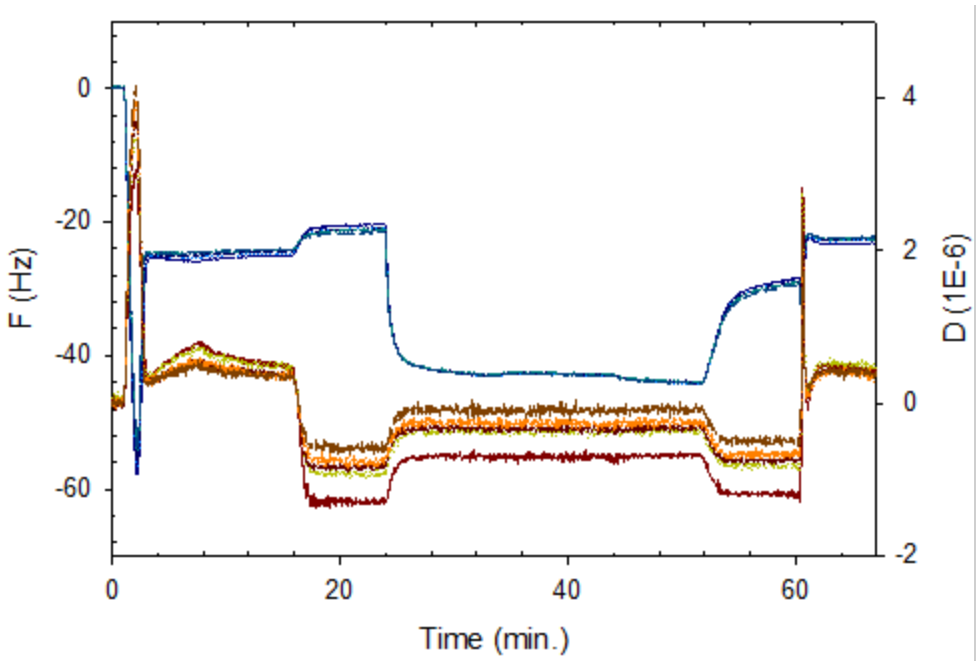

Figure 1.3 Formation of a PC bilayer on SiO_2 crystal. After bilayer formation, buffer flows through the module remove un-ruptured or excess vesicles. Water is introduced followed by the PMA solution. AuNPs diluted with PMA are introduced followed by PMA solution and a water rinse. Buffer is introduced last to complete the experiment. Blue lines represent the frequency fort each overtone and red lines represent dissipation fort each overtone. Overtones 3, 5, 7, 9 and 11 are shown on the plot. (Buffer rinse 6:20; water rinse 14:37; PMA solution 22:53; AuNP/PMA 32:12; PMA solution 42:30; water rinse 50:47; buffer rinse 59:23

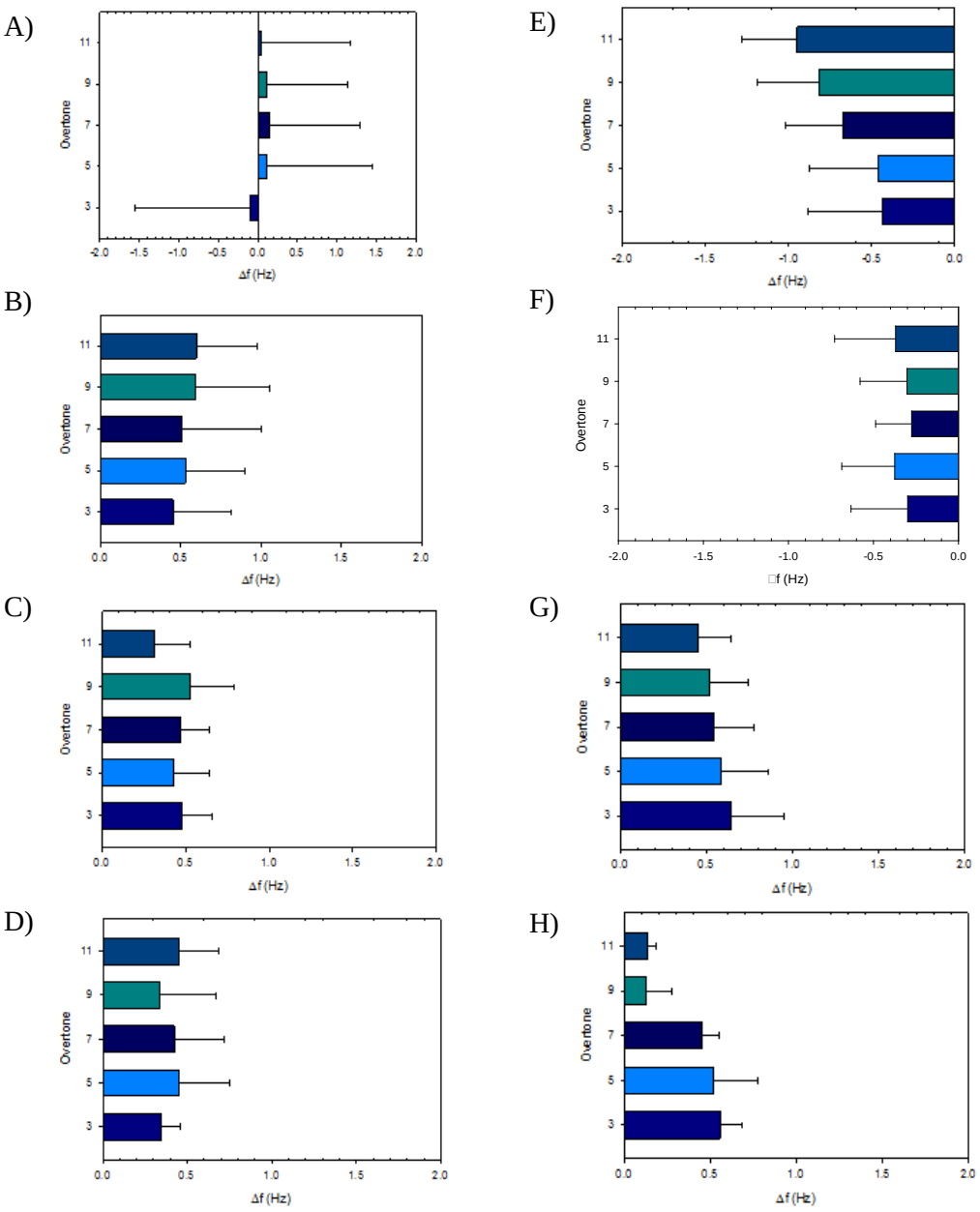

Figure 1.4 Analysis of the frequency change at each overtone for the comparison of AuNPs diluted in de-ionized water and diluted in PMA solution, respectively. Frequency change is a result of nanoparticle introduction and interaction with PC bilayer. A) 2 nm AuNP/H_2O, B) 5 nm AuNP/H_2O, C) 10 nm AuNP/H_2O, D) 40 nm AuNP/H_2O, E) 2 nm AuNP/PMA, F) 5 nm AuNP/PMA, G) 10 nm AuNP/PMA and H) 40 nm AuNP/PMA.

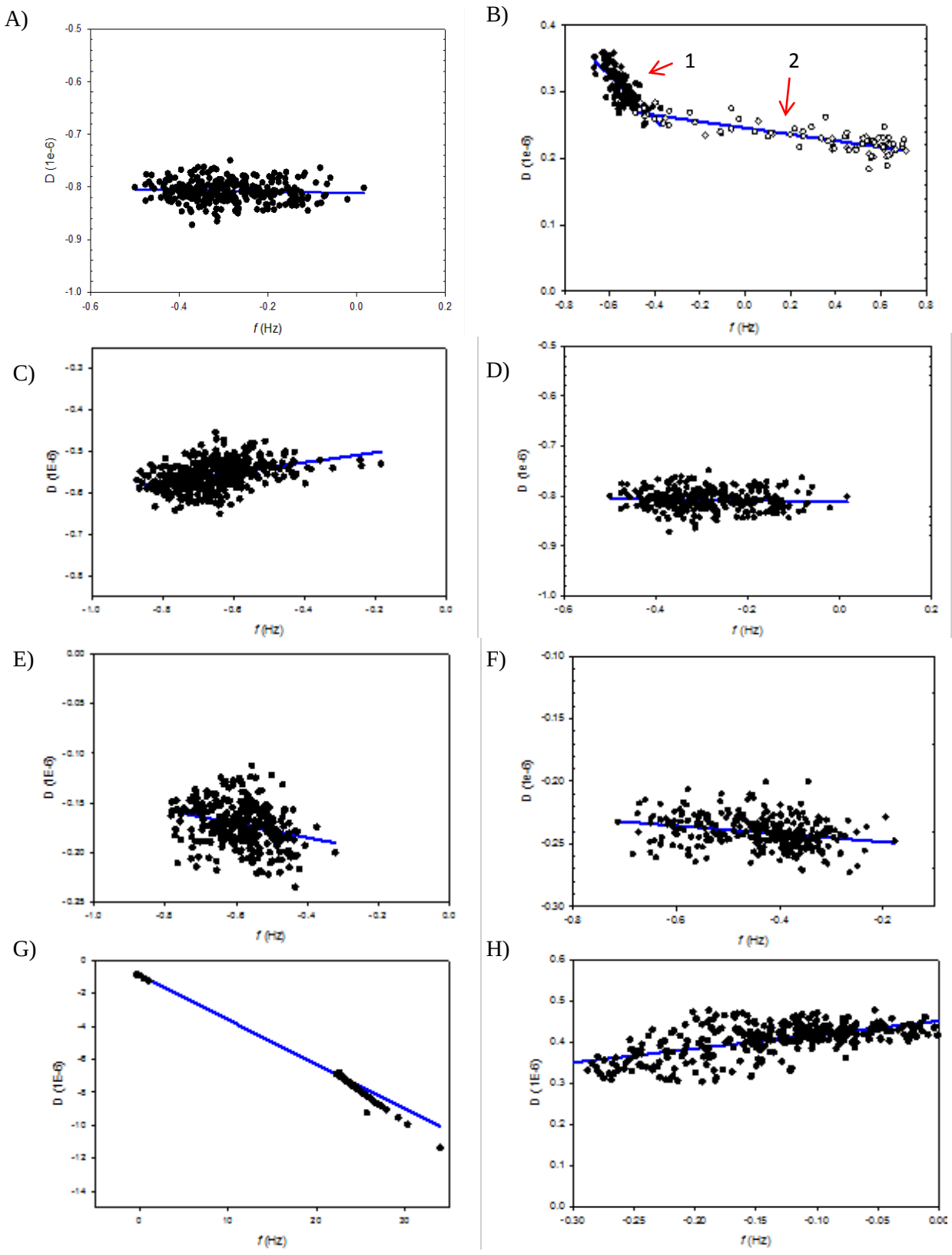

Figure 1.5 Dissipation versus frequency plot at the 7th overtone for AuNPs diluted in PMA interacting with the PC bilayer. The plot illustrates the D/*f* value for nanoparticle introduction over the course of 10min. A) 2 nm AuNP/H_2O, B) 2 nm AuNP/PMA, C) 5 nm AuNP/H_2O, D) 5 nm AuNP/PMA, E) 10 nm AuNP/H_2O, F) 10 nm AuNP/PMA, G) 40 nm AuNP/H_2O and G) 40 nm AuNP/PMA

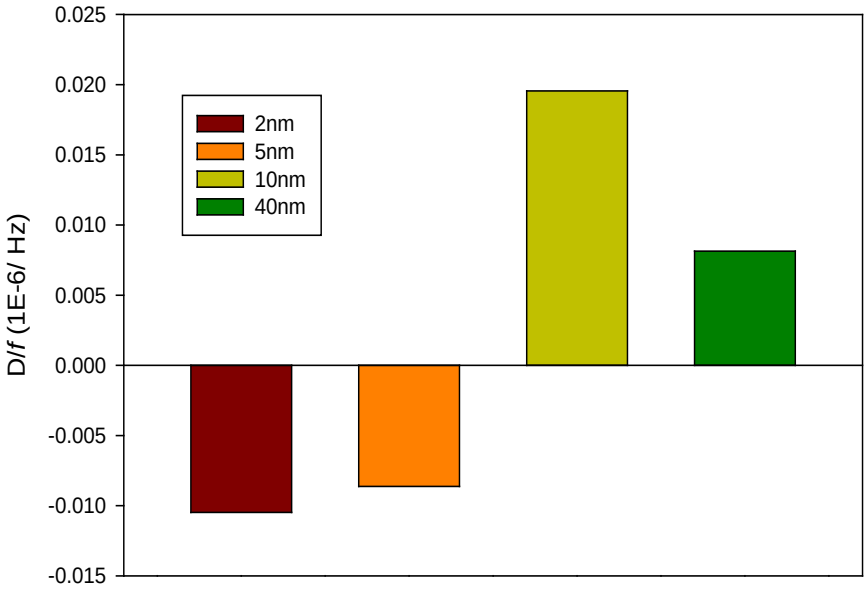

Figure 1.6 Comparison of D/f at the 7th overtone for 2, 5, 20 and 40 nm Bare Gold NPs diluted in PMA solution. D/f corresponds to membrane rigidity. D/f values were obtained 5 minutes after nanoparticle introduction. Nanoparticles were run for a total of 10 min.

Chapter 1 References

1. Jarvie, H.P., Al-Obaidi, H., King, S.M., Bowes, M.J., Lawrence, M.J., Drake, A.F., Green, M.A. Dobson, P.J. Fate of silica nanoparticles in simulated primary wastewater treatment. Environ. Sci. Technol. 2009; 43:8622-8628.
2. Kaegi, R., Ulrigh, A., Sinnet, B., Vonbank, R., Wichser, A., Zuleeg, S., Simmler, H., Brunner, S., Vonmont, H., Burkhardt, M., Boller, M. Synthetic TiO_2 nanoparticle emission from exterior facades into the aquatic environment. Environ. Pollution. 2008;156:233-239.
3. Diegoli, S., Manciulea, A.L., Begum, S., Jones, I.P., Lead, J.R., Preece, J.A. Interaction between manufactured gold nanoparticles and naturally occurring organic molecules. Sci. Total Environ. 2008;402:51-61.
4. Chen, K.L., Elimelech, M. Influence of humic acid on the aggregation kinetics of fullerene (C_{60}) nanoparticles in monovalent and divalent electrolyte solutions. J. Colloid and Interface Sci. 2007;309:126-134.
5. Thomas, C.R., x George, S., Horst, A.M., Ji, Z., Miller, R.J., Peralta-Videa, J.R., Xia, T., Pokhrel,S., Mädler, L., Gardea-Torresdey, J.L., Holden, P.A., Keller, A.A., Lenihan, H.S., Andre E. Nel, A.E., Zink, J.I. Nanomaterials in the environment: From materials to high-throughput screening to organisms. ACS nano; 2011:5:1:13-20.
6. Li, M., Huang, C.P. Stability of oxidized single-walled carbon nanotubes in the presence of simple electrolytes and humic acid. Carbon. 2010; 48:4527-4534.
7. Domingos, R.F., Tufenkji, N., Wilkinson, K.J. Aggregation of titanium dioxide nanoparticles: Role of fulvic acid. Environ. Sci. and Tech. 2009; 43:1282-1286.
8. Gao, J., Powers, K., Wang, Y., Zhou, H., Roberts, S.M., Moudgil, B.M., Koopman, B., Barber, D.S. Influence of suwannee river humic acid on particle properties and toxicity of silver nanoparticles. Chemosphere. 2012; 89:96-101.
9. Hou, W.C., Moghadam, B.Y., Corredor, C., Westerhoff, P., Posner, J.D. Distribution of functionalized gold nanoparticles between water and lipid bilayers as model cell membranes. Environ. Sci. and Tech. 2012; 46:1869-1876.
10. Ginzburg, V.V., Balijepalli, S. Modeling of thermodynamics of the interaction of nanoparticles with cell membranes. Nano Letters. 2007; 7:12:3716-3722.
11. Barenholz, Y., Gibbes, D., Litman, B.J., Goll, J., Thompson, T.E., Carlson, F.D. A simple method for the preparation of homogenous phospholipid vesicles. Biochem. 1977; 16:12:2806-2810.
12. Keller, C.A., Glasmastar, K., Zhdanov, V.P., Kasemo, B. Formation of supported membranes from vesicles. Physical Review Letters. 2000; 84:23:5443-5446.
13. Mechler, A., Praporski, S., Atmuri, K., Boland, M., Separovic, F., Martin, L.L. Specific and selective peptide-membrane interactions revealed using quartz crystal microbalance. Biophysical Journal. 2007; 93:3907-3916.
14. Nason, J.A., McDowell, S.A., Callahan, T.W. Effects of natural organic matter type and concentration on the aggregation of citrate-stabalized gold nanoparticles. J. Environ. Monitoring. 2012; 14:1885-1892.

15. Bothun, G. Hydrophobic silver nanoparticles trapped in lipid bilayers: Size distribution, bilayer phase behavior and optical properties. J Nanobiotech. 2008; 6:13.
16. Ghosh, S., Jiang, W., McClements, J.D., Xing, B. Colloidal stability of magnetic iron oxide nanoparticles: Influence of natural organic matter and synthetic polyelectrolytes. Langmuir. 2011; 27:8036-8043.
17. Park, S.H., Oh, S.G., Mun, J.Y., Han, S.S. Loading of gold nanoparticles inside the DPPC bilayers of liposome and their effects on membrane fluidities. Colloids and Surfaces B: Biointerfaces. 2006; 48:112-118.
18. Hook, F., Ray, A., Norden, B., Kasemo, B. Characterization of PNA and DNA immobilization and subsequent hybridization with DNA using acoustic-shear-wave attenuation measurements. Langmuir. 2001; 17:8305-8312
19. Feiler, A.A., Sahlholm, A., Sandberg, T., Caldwell, K.D. Adsorption and viscoelastic properties of fractionated mucin (BSM) and bovine serum albumin (BSA) studied with quartz crystal microbalance (QCM-D). J. Colloid and Interface Sci. 2007; 315:475-481.
20. Moh, K.M., Ho, X., Su, X. DNA assembly on streptavidin modified surface: A study using quartz crystal microbalance with dissipation and resistance measurements. Sensors and Actuators B. 2008; 131:371-378.
21. Rodahl, M., Hook, F., Fredriksson, C., Keller, C.A., Krozer, A., Brzezinski, P., Vionova, M., Kasemo, B. Simultaneous frequency and dissipation factor QCM measurements of biomolecular adsorption and cell adhesion. Faraday Discuss. 1997; 107:229-246.
22. Frost, R., Coue, G., Engbersen, J.F.J., Zach, M., Kasemo, B., Svedhem, S. Bioreducible insulin-loaded nanoparticles and their interaction with model lipid membranes. J. Colloid and Interface Sci. 2011; 362:575-583.
23. Fiedler, S.L., Violi, A. Simulation of nanoparticle permeation through a lipid membrane. Biophysical J. 2010; 99:144-152.
24. Tedesco, S., Doyle, H., Blasco, J., Redmond, G., Sheehan, D. Oxidative stress and toxicity of gold nanoparticles in Mytilus edulis. Aquatic Toxicity. 2010; 100:178-186.
25. Cremer, P.S., Boxer, S.G. Formation and spreading of lipid bilayers on planner glass supports. J. Phys. Chem. B. 1999; 103:2554-2559.

Chapter 2

Chapter 2: Determining the Effect of Chemically Functionalized AuNPs with a SLB in the Presence of Humic Acid Using a QCM-D

2.1 Abstract

The introduction of nanoparticles into the environment and subsequently the food chain is swiftly becoming a problem due to the mass production of nano-engineered products, as knowledge and technology continues to boom. Presently, about 2300 tons of nanoparticles are being manufactured and estimated to reach 58000 tons by 2020[1]. The rapid production and vast array of materials used has peaked research in determining the possible toxic effects of these nano-materials. Most research has been focused on the chemical composition of the materials; however, this study was aimed at determining the mechanistic interaction associated with the physical properties of the nano-materials. In this study a model cell membrane composed of L-α-phosphatidylcholine (egg PC) was used to test different functionalized 12 nm gold nanoparticles (1-propanethiol, 2-mercaptoethanol, 2-aminoethanethiol and 3-mercaptopropionic acid) in order to determine the interaction of nanoparticles with the bilayer. The high risk of nanoparticle release into the environment has led to the use of humic acid (HA), a naturally occurring polymer typically found in both aquatic and soil systems, in order to mimic conditions found environment. The quartz crystal microbalance with dissipation (QCM-D) was used to monitor the interactions of the nanoparticles with the supported lipid bilayer (SLB) by taking measurements of the frequency (*f*) and dissipation (D), which relate to mass and conformational changes in the adsorbed film. Several overtones associated with *f* and D, allowed for theoretical interpretation of changes in different layers of the SLB. Functionalized AuNPs were shown to decrease the rigidity of the lipid bilayer by increasing the dissipation and decreasing the mass associated with the adsorbed film (SLB). The presence of humic acid stabilized the nanoparticles and provided increased electrostatic repulsion which resulted in decreased mass losses from the membrane and much smaller decreases in membrane rigidity. It was

concluded that presence of humic acid reduces the effects of functionalized nanoparticle interaction with a lipid bilayer. These results may mean that natural organic matter has the ability to reduce the cytotoxic effects of nanoparticles released into the environment. The ability to determine the toxic physical properties and mechanisms by which nanoparticles interact with lipid bilayers coupled with the knowledge that natural organic matter may alter the toxicity will greatly aid in development of non-toxic nano-materials.

2.2 Introduction

Nanoparticles have gained much attention in the past decade due to the rapid growth in nanotechnology, which has driven diverse application and development of new nanoparticles[2]. The advancements made in nanotechnology and engineered nanoparticles frequently incorporated into consumer and industrial products has heightened the importance of understanding the impact these materials may have on humans and the environment[3]. Research has estimated that the emissions of nanoparticles into the environment will increase drastically in the future due to development and use in consumer products reinforcing the importance of evaluating the risks associated with environmental contact[4]. Due to consumer and industrial use coupled with manufacturing, the inevitable release into the environment is likely through both direct discharges and industrial and domestic wastewater effluents[5]. A recent study has shown that concentrations of up to 0.7 μg/ L of synthetic TiO_2 nanoparticles from urban applications were being released into aquatic environments, with much higher concentrations seen in the effluent of wastewater treatment facilities[6]. The presence of these particles in the natural environment has the potential to cause harmful effects on different aquatic life as well as plants and crops used for both human and livestock consumption[7-10].

Nanoparticles released into the environment are likely to encounter natural organic matter present in all environmental systems, from aquatic to soil. It has been found in many studies using different nanoparticles, that natural organic matter has the capacity to stabilize the colloidal solution against aggregation through electrostatic repulsion[11]. Since aggregation has been found to be one of the primary

controlling factors of transport and toxicity for nanoparticles in the environment, it is of utmost importance to study the interaction and influence of natural organic matter on nanoparticle aggregation[5,11-14]. The adsorption of natural organic matter onto the surface of nanoparticles can have dramatic impacts on particle dispersion which results in altering the fate and transport of particles as well as the bioavailability and toxicity of this nano-material[5]. Most NOM contains large amounts of carboxyl and phenolic –OH groups which if adsorbed to the surface of nanoparticles will impart a negative charge[31]. The charge modification enhances the stability of the aqueous nanoparticle solution through repulsive electrostatic forces[13].

Several studies have been done which showed that humic acid aided in the stabilization of nanoparticle solutions by preventing aggregation[12]. Humic acid has been considered to be the most important natural organic colloid and despite its complex and heterogeneous composition it has been extensively studied and characterized[12]. The adsorption of humic acid onto the surface of nanoparticles changed the charge, heterogeneity of the charge and steric repulsion[12]. Therefore, nanoparticle interaction with lipid membranes which caused morphology changes in the membrane can be attributed to the charge, composition and size of the interacting NP[15]. Morphological reorganization and hole formation in lipid bilayers which are strongly dependent on the surface hydrophobicity/hydrophilicity of the interacting nanoparticles[15] may be attributed to changes in the surface characteristics caused by the adsorption of natural organic matter to the nanoparticle surface.

Nanoparticle interaction with cell membranes and cytotoxicity has been studied extensively with regards to the chemical property of the materials used. Lin et al has shown that TiO_2 nanoparticles in the presence of dissolved humic acid were prevented from adhering to algal cells by increased electrostatic repulsion, ultimately decreasing the toxic effects of the TiO_2 nanoparticles[14]. In vitro studies utilizing cultured cells have typically been used to predict the cytotoxic responses of a broad range of compounds[16]. The simple assays used colorimetric and fluorescent dyes to assess membrane integrity or cell metabolism. Unfortunately, these assays have proven to be unreliable in the assessment of nanoparticle cytotoxicity[16]. Bacterial cells were tested through deposit on hydrophobic nanoparticle

coated surfaces in order to test effects associated with polarity, which caused the bacterial membrane to become soft[17]. Physicochemical factors, specifically size, surface charge density and polarity have been linked to the ability of the nanoparticles to strongly interact with cell membranes[18]. Studies have shown that strong membrane interaction resulted in either adsorption to the membrane or compromised the membrane integrity resulting in the formation of holes[18]. The resulting morphology was therefore dependent on the size and surface charge of the nanoparticle rather than the biochemical properties of the material. It can be concluded that the mechanism of cell membrane disruption was therefore, a consequence of purely physical characteristics of the nanoparticles.

Figure 1 provides a schematic description of the various modes of nanoparticle membrane interaction and the mechanisms by which lipid membrane disruption may occur. Nanoparticles are thought to have the ability to adsorb to the surface, partially or completely solubilize into the hydrophobic interior of the lipid chains (Figure 1A). As a consequence of these types of nanoparticle interactions with the membrane, the molecular packing of the bilayer becomes disrupted. The lipid chains respond to this disruption by stretching in order to maintain the molecular space filing requirement of the lipid bilayer and eliminate voids. Membrane thinning and chain stretching are energetically unfavorable processes, which at a critical nanoparticle dosage, may result in the formation of cylindrical pores (Figure 1B,C). Two types of pores may be possible including one seen in Figure 1B where the pore walls are lined with the nanoparticles or in Figure 1C, where a toroidal pore has formed in which both lipids and nanoparticles make up the pore wall. Under certain conditions of increased strain on the membrane due to nanoparticle interaction, membrane lysis may occur leading to the formation of lipid/nanoparticle aggregates (Figure 1D). At the critical nanoparticle dosage where the membrane may experience physical changes, we can conclude that the structural integrity of the membrane has been compromised.

Interpreting the impacts of nanoparticles on environmental systems will facilitate in the design of non-toxic materials and improve manufacture, use and disposal of these products in order mitigate possibly toxic environmental conditions[11]. The use of knowledge gained from techniques that are able to determine the potential toxic properties of nanoparticles will aid in the design and synthesis of new

nanoparticles that have been modified to reduce or eliminate toxicity[3]. Although many studies have been published regarding the toxicity of nanoparticles to cells, the nature of cytotoxicity associated with the "nano-specific" (physical) properties of the nanoparticle and the mechanisms by which toxicity occurs is still not well understood. Therefore, the goal of this research was to provide a fundamental way in which to quantify size related nanoparticle toxicity under sterile lab and environmental conditions. The purpose was to be able to determine if mechanistic interactions were modified and cytotoxicity was quantitatively altered by the presence of natural organic matter. In this study humic acid (HA) was used in order to simulate the conditions found in the environment. The application of gold nanoparticle (AuNP) in diagnostic and drug delivery has increased greatly due to their versatility in size, shape and functionalization[19]. Gold nanoparticles were chosen for this study because of their frequent use in vivo and the nontoxic properties of the bulk metal.

2.3 Materials

Spherical, 12nm diameter gold nanoparticles were purchased from Nanopartz Inc. (Loveland, CO) and were functionalized with 1-propanethiol, 2-mercaptoethanol, 2-aminoethanethiol and 3-mercaptopropionic acid. The results were compared to a 12nm bare gold nanoparticle, purchased from the same company. Zeta potentials were given by the manufacturer shown in Table 1. The original stock solutions were dispersed in de-ionized water, stabilized with citrate and stored at 7°C in a light impenetrable container. The concentrated nanoparticle solutions were diluted with de-ionized or the humic acid solution to a concentration of 3.119×10^{12} particles/ mL.

Humic acid was purchased from Aldrich (St. Louis, MO). The polymer solution was prepared by adding 0.1 g of humic acid powder to 1000 mL of de-ionized water and stirred for 1 h at 600 rpm on a stir plate (VWR, Arlington Heights, IL). The solution was then sonicated for 1 h in a water bath ultrasonic cleaner (Bransonic, Danbury, CT) to yield a concentration of 100 mg/ L and stored at 7°C in a light impenetrable container to preserve integrity.

L-α-phosphatidylcholine (egg, chicken) (PC) with purity > 99% was purchased from Avanti polar lipids. 1 g of egg PC powder was solubilized in 10 mL of ethanol to yield a 100 mg/mL solution stored at -20 °C. Other chemicals were purchased from Sigma-Aldrich (St. Louis, MO).

A buffer solution made of 10 nM Tris (hydrozymethyl) aminomethane with ≥ 99.9% purity and 100 nM sodium chloride, +80 mesh particle size, pH 7.8, was prepared in de-ionized water.

QCM-D sensor crystals (5 Hz), reactively sputter-coated with silicon dioxide, were purchased from Biolin Scientific (Gothenburg, Sweden). Crystals were cleaned using modified Qsense protocols which include an ethanol rinse followed by de-ionized water then 2% sodium dodecyl sulfate rinse. The crystals are then rinsed in de-ionized water again and dried with nitrogen gas. To remove any other organic contaminants and slightly oxidize the sensor surface, the crystals undergo two cycles of 45 s oxygen plasma cleaning using Plasma Prep II (SPI Supplies, West Chester, PA). Under favorable conditions the sensor crystals can be used up to 10 times.

2.4 Methods

2.4.1 SLB Formation

An egg PC solution vesicle solution (previously described) was made and stored under nitrogen at 7°C for up to one month's time. It is recorded that the solution was viable for up to 6 months[20]. However, after one month's time it was found that bilayer formation no longer occurred. Before use, lipid vesicle solutions were diluted to 0.1 mg/ mL if not otherwise stated. All stock and dilute solutions were votexted for 15 s prior to use.

2.4.2 QCM-D

QCM-D measurements were performed with the Q-sense E4 system (Biolin Scientific, Sweden). Thin quartz discs sandwiched between two gold electrodes were placed in the four flow modules of the QCM-D. The sensors were then exposed to different solutions continuously delivered (flow rate of 0.15

mL/min unless otherwise stated) by the aid of a peristaltic pump (IPC high precision multichannel dispenser, ISMATEC, Switzerland).

The QCM-D is an acoustic technique which allows for the detection of mass and thin film property changes of thin films adsorbed to the sensor surface. The piezoelectric properties of the quartz sensor crystal allow for excitation of the sensor through AC voltage oscillation across the electrodes. The QCM-D then interprets the changes in oscillations as frequency (mass changes) and dissipation (film viscosity changes), which were associated with mass variations in the adsorbed film. The Suaerbrey equation for rigid films determines the inverse relationship between mass adsorption and frequency change, with mass sensitivity constant $C = 17.7\ ng \cdot cm^{-2} \cdot Hz^{-1}$ for 5 MHz sensor crystals,

$$\Delta m = -\frac{C \cdot \Delta f}{n}$$

where an increase in mass is directly proportional to a decrease in frequency. Energy dissipation changes are associated with the rigidity of the adsorbed film. The normal mass and dissipation sensitivities of QCM-D measurements in liquid are ~1.8 ng/cm^2 and ~0.1 x 10^{-6}, respectively.

Changes in the dissipation and normalized frequency of the third, fifth, seventh, ninth and eleventh overtone ($n = 3, i.e., 15MHz$) are presented.The third through eleventh harmonics of the sensor crystal's natural frequency (5 MHz) were measured and normalized automatically to each overtone (f/n, where f is frequency and n is the harmonic number) by the Q-Sense software. The fundamental frequency was not analyzed due to its highly sensitive nature to changes in the bulk solution during flow[6].

2.4.3 Functionalized Nanoparticle/H2O Interaction with SLB

QCM-D sensors were cleaned according to adapted manufacturer protocols. The sensors were calibrated in air and Tris-NaCl buffer for both frequency and dissipation by determining the natural frequency and dissipation for each overtone and crystal, which differ slightly as the crystal ages, in order to establish a baseline. All solutions delivered to the crystals used the same flow rate (0.15 mL/min) via a peristaltic pump (IPC high precision multichannel dispenser, ISMATEC, Switzerland). A stable lipid

bilayer was formed within 6 min of flowing the PC vesicle solution over the sensor surface. Sensors/SLB were then rinsed to remove un-ruptured vesicles. A baseline was then established in de-ionized water to prevent complications with viscosity changes associated with different solutions. Functionalized AuNPs diluted in de-ionized water were washed over the membrane for 10 min. The SLB was then rinsed in de-ionized water and Tris-NaCl buffer respectively. Experiments were run in triplicates for each species of nanoparticle.

2.4.4 Functionalized AuNP/Humic Acid Interaction with SLB

Experiments were also performed in the presence of a humic acid solution which was introduced 8 min before and post the introduction of the AuNPs/HA solution in the chamber. The AuNP/HA solution used in this section was diluted to 3.119×10^{12} particles/mL with 100 mg/L humic acid solution before being introduced into the module chamber. All other aspects of the procedure remained the same except replicates performed ranged from 6-12 per type of functionalized nanoparticle.

2.4.5 Data Analysis

The data used to determine nanoparticle toxicity was compiled from plots and data sets produced by the QCM-D. As noted above, two different experiments were performed; 1) functionalized gold nanoparticles diluted in water, 2) functionalized gold nanoparticles diluted in humic acid. Plots representing raw data taken from the QCM-D showed ~ 20 min time lapse between the time when nanoparticles diluted in water were added and the time when the nanoparticles diluted in humic acid were introduced. This was directly related to the necessity of stabilizing the system to the viscosity reminiscent of the nanoparticle solution (i.e. the solution used to diluted the nanoparticles, either de-ionized water or humic acid).

The comparison of Δf at the six different overtones (3, 5, 7, 9 and 11) was compiled and averaged for each overtone according to the number of replicates performed for each functionalized AuNP. Frequency changes were recorded at one minute before changing over to functionalized AuNP and humic

acid solution and one min before changing back to de-ionized water from humic acid solution. For the control experiments (AuNPs in water with no humic acid added) frequency changes were recorded at one min before changing into the AuNP/H_2O solution and at one minute before changing into buffer from de-ionized water. Standard deviation values were taken from the frequency change data and used to produce bar charts highlighting the difference in frequency change between each overtone, which provides information on adsorption/desorption to/from the lipid bilayer.

Plots of D/f vs. functionalized AuNP were made in order to observe the change in viscoelastic properties per mass change for each type of functionalized AuNP. Averaged values for D and f were taken at one minute before AuNP solution introduction into the chamber (i.e. changing from humic acid into NP/humic solution) and one minute before de-ionized water rinse (i.e. changing from humic acid into de-ionized water). The D and f plots should provide insight on viscosity changes of the SLB associated with AuNP interactions with the supported lipid bilayer.

2.5 Results

2.5.1 Raw QCM-D Data Plots

Figure 2.1 represents a QCM-D plot for an experiment performed with AuNPs diluted in de-ionized water. Bilayer formation was monitored by observing the changes associated with frequency and dissipation corresponding to the blue and red lines, respectively. The large changes in frequency and dissipation within the first 6 min of the experiment correspond to bilayer formation. The membrane was then stabilized in Tris-NaCl buffer, depicted in the horizontal slope of both D and f from 8 to about 15 min. The small increase in frequency accompanied by the large decrease in dissipation illustrates the change over from buffer to de-ionized water, then into the NP and de-ionized water solution, and consequently back to water. At ~42 min, an appreciable drop in frequency and significant increase in dissipation was observed, as a result of Tris-NaCl buffer introduction.

Figure 2.2 shows a typical QCM-D plot for the interaction of AuNPs, in the presence of humic acid, with the supported lipid bilayer. This plot was similar to Figure 2.1, although, 16 min are added to

the overall experimental procedure due to the introduction of the humic acid solution before and after the introduction of the NP/humic acid solution. Nanoparticle interactions are not obvious at this scale, but small changes in the dissipation and frequency are occurring.

2.5.2 Effect of Functionalized Nanoparticles Diluted in De-ionized Water on Membrane Interaction

The nanoparticles used in the study (12 nm AuNP, 1-propanethiol Au, 2-mercaptoethanol Au, 2-aminoethanethiol Au and 3-mercaptopropionic acid Au) were diluted in water and then plotted for their interaction with a SLB. As show in Figure 2.3, the 12nm AuNP, 1-propanethiol Au, 2-mercaptoethanol Au and 2-aminoethanethiol Au nanoparticles had similar interactions with the membrane, seen as ~ 0.5 Hz increase in frequency for each overtone. The 12 nm AuNPs had a significant increase in frequency for overtones 3 and 5, although the 5^{th} overtone was slightly higher than the 3^{rd} overtone for frequency change (Figure 2.3A). For the 12 nm AuNPs, the changes in frequency appear to decrease with increasing overtone, the 11^{th} overtone having the smallest appreciable Δf. The 1-propanethiol functionalized AuNP had large changes in frequency (~ 0.7 Hz) for overtones 5 and 9 and smaller changes in frequency (~ 0.6 Hz) for overtones 3, 7 and 11 (Figure 2.3B). The 2-mercaptoethanol AuNPs interaction with the SLB resulted in a nearly symmetrical change in frequency seen for each overtone (Figure 2.3C). Overtone 5 for this functionalized nanoparticle has a slightly lower Δf (~ 0.5 Hz) than the other 4 overtones (Δf ~ 0.6 Hz). 2-aminoethanethiol AuNPs had a similar to trend to the 2-mercaptoethanol AuNPs, with equal changes frequency for each overtone. However, the 11^{th} overtone for 2-aminoethanethiol AuNPs was slightly lower Δf of ~ 0.5 Hz (Figure 2.3D). The AuNP functionalized with 3-mercaptopropionic acid had a much smaller increase in frequency of ~ 0.2 Hz for each of the 5 overtones represented, which was vastly different than the responses of the other nanoparticles (Figure 2.3E). For 3-mercaptopropionic acid, the overtones associated with the hydrophobic region of the bilayer (overtone 7 and 9) have slightly larger increases in Δf than the other overtones recorded.

2.5.3 Effect of Functionalized Nanoparticles Diluted in Humic Acid on Membrane Interaction

The functionalized nanoparticles used in the study were subjected to simulated environmental conditions through the addition of humic acid to the nanoparticle solution. The results of the interaction of the nanoparticles under these conditions can be seen in Figure 2.3 F–J. All the nanoparticles, except for the 3-mercaptopropionic acid, interacted with the membrane through a positive change in frequency. The 2-aminoethanethiol and 2-mercaptoethanol interacted very similarly with an increase in frequency of ~ 0.3 - 0.4 Hz across each of the five overtones. The 12 nm bare gold nanoparticles and 1-propanethiol functionalized Au nanoparticles showed similar small increases in frequency. However, the 1-propanethiol AuNPs interaction with the SLB was minimal. The 12 nm bare AuNP showed a significant increase in frequency, limited to region of the bilayer associated with the 5^{th} and 7^{th} overtone. The results for 3-mercaptopropionic acid presented much different results from the rest of the nanoparticles, with a decrease in frequency, which was marginally larger for overtones 9 and 11.

2.5.4 Membrane Conformational Changes in Relation to D vs. f

The viscoelastic changes per coupled unit of mass (D/f) were performed for each of the functionalized nanoparticles diluted in de-ionized water or humic acid. Figure 2.4 highlights the results obtained from the D/f data. All the plots were very similar in nature, with an almost horizontal slope indicating very small changes in the dissipation given slightly larger positive changes in frequency. Each graph had very tightly packed data points, which were nearly indistinguishable from one another in the plots. There were not any appreciable changes between AuNPs diluted in de-ionized water or AuNPs diluted in humic acid.

2.5.5 Nanoparticle Chemical Functionality and SLB Structure Correlation

The D/f value was calculated by obtaining the dissipation and frequency data for the 7th overtone (theoretical middle layer of the bilayer) 5 min after nanoparticle introduction to the SLB for each nanoparticle diluted in de-ionized water and humic acid. Figure 2.5 directly compared the data points and provided a clear overview of each nanoparticle at both system conditions. A clear trend in the data was observed for each nanoparticle species, although 3-mercaptopropionic acid does not follow this trend. The trend showed that the nanoparticles diluted in de-ionized water had a slightly lower D/f in comparison to the same nanoparticle species in humic acid. While 2-mercaptoethanol followed this same trend, it had a very uncharacteristically large negative value for D/f when diluted in water. The corresponding D/f value for this nanoparticle in humic acid was significantly smaller than the other AuNPs, but was positive in value as per the trend. The 3-mercaptopropionic acid had a much larger, positive D/f value for the AuNPs diluted in de-ionized water in comparison to the same particles in humic acid.

2.6 Discussion

2.6.1 Membrane Destabilization as a Function of Nanoparticle Functionalization

It is well known that the QCM-D has the capability of detecting nano-scale mass changes associated with the crystal sensor surface in relation to the five overtones examined in this study. The changes in Δf (mass) associated with each overtone were depicted in Figure 2.3, which illustrates the data collected for each functionalized nanoparticle diluted in de-ionized water and humic acid. The use of the plots allow for the quantification of mass change and the theoretical interpretation of the mechanism by which mass change occurred. Changes in frequency at the membrane surface were associated with overtones 3 and 5, whereas the 9th and 11th overtone relate more closely to the crystal sensor surface where a layer of water was trapped by the lipid bilayer formation. Studying mass loss specifically, it can be seen in Figure 2.3 plots A-E, the nanoparticles diluted in water all had significant mass losses

associated with each of the five overtones studied. It would appear that mass losses were nearly independent of functionalization as the 12 nm bare gold nanoparticle experienced equivalent losses in mass compared to the functionalized nanoparticles, save 3-mercaptopropionic acid AuNP. Given these observations it can be concluded that mass losses were attributed to nanoparticle properties other than functional group, such as size, polarity or charge in relation to membrane interactions. Properties of the 12 nm gold nanoparticles were listed in Table 1.

Reviewing the properties of the 12 nm AuNPs, each nanoparticle had a largely negative zeta potential despite the charge or lack of charge known for the particular NP. It was known that the length of the ligand (functional) group attached to the nanoparticle affects the zeta potential of the particle. The ligand groups attached to the 12 nm AuNPs in this study were very short, which resulted in the zeta potential of the NP material dominating the overall zeta potential measured. It was highly possible, that given the negative charge of the particles and the zwitterionic charge of the PC lipid bilayer, the nanoparticles were able to remove mass from the membrane by attaching to and then lifting away lipids in the process of flowing across the membrane surface. The mass losses seen in Figure 2.3 A-E, extended from the surface of the membrane equally through to the surface of the sensor crystal. This was possibly due to lipid loss from the membrane surface which would result in membrane rearrangement and contribute to losses in mass associated with the surface of the membrane. Hydration trapped at the sensor surface and now able to escape due to gaps created in the membrane may have contributed to the mass losses seen at the sensor crystal surface. It seemed odd that the hydrophobic 1-propanethiol AuNP diluted in de-ionized water did not add mass to the SLB, but instead removed mass. This can be attributed to the 12 nm diameter of the nanoparticle, as it was known that the PC lipid bilayer was 5 nm in width and previous studies have shown that nanoparticles must not be larger in diameter than the width of the membrane[22,23]. Therefore, mass removal was likely caused by electrostatic interaction with the zwitterionic surface of SLB because of the negative charge exhibited by the nanoparticle, and during NP/SLB interaction, the shear forces from fluid flow caused the nanoparticle to be removed from the membrane taking attached lipid groups with it[2]. This mechanism applied to the 12 nm bare AuNP, 2-

mercaptoethanol and 2-aminoethanthiol as well. The 3-mercaptopropionic acid appears to have a different mechanism or exhibits a much weaker electrostatic interaction with the zwitterionic SLB due to the significantly smaller mass loss (Figure 2.3E).

The nanoparticles diluted in humic acid had a considerably small interaction with the supported lipid bilayer illustrated by the small amount of mass lost for the 12 nm AuNP, 1-propanethiol AuNP, 2-mercaptoethanol AuNP and 2-aminoethanethiol AuNP. Humic acid has been found to adsorb to the surface of nanoparticles leading to increased steric repulsion between nanoparticles in solution, resulting in a more stabilized nanoparticle suspension[6,11,14]. It was found in one study that both nanoparticles dissolved in HA and surface-bound with HA were from adhering to the surface of algal cells due to the increased steric repulsion[14]. The results from this study explain why the interaction of the functionalized nanoparticles with the SLB was greatly reduced in the presence of humic acid. The 12 nm and 1-propanethiol AuNPs appear to be much more effected by the presence of HA as their interactions are significantly smaller than the other three nanoparticles used in this study. The 1-propanethiol may have the smallest mass reduction when HA is present because of the hydrophobic nature of the functional group. The hydrophobicity of the functional group did not allow the nanoparticle to remove hydration from the membrane and coupled with high steric repulsion it was not able to come into contact with the membrane. The slightly larger amount of mass removed from the membrane seen with the 12 nm AuNP in comparison to the 1-propanethiol may be due to it hydrophilic nature. Mass losses, although small, were concentrated near the surface of the membrane meaning lipid and/or hydration was removed. The AuNPs functionalized with 2-mercaptoethanol and 2-aminoethanethiol had equal amounts of mass removed, nearly uniformly for each overtone. The humic acid has stabilized the nanoparticle solution by adsorbing and coating the nanoparticles thereby reducing or eliminating the chance of nanoparticle aggregating and increasing steric repulsion between the nanoparticles and the membrane which was also charged. The decrease in the amount of mass removed by half may be attributed to the increase in charged repulsion. 3-mercaptopropionic acid had the most unusual interaction with the membrane when in the presence of humic acid by adding a small uniform amount of mass across the width of the lipid bilayer.

Given that the mass increase appears to be larger with increasing overtone it may be that a minimal number of nanoparticles were able to adsorb to the surface of the membrane and the mechanism of adsorbing caused conformational changes in the membrane allowing for hydration to enter the membrane and by the hydrophilic nature of the water molecule accumulated nearest the crystal surface.

2.6.2 Membrane Conformational Changes in Relation to D vs. f

The comparison of dissipation to frequency values obtained from the QCM-D provided information about the change in conformation of the membrane given the mechanism of mass adsorption/desorption. The elimination of time from the plot enabled the ratio of dissipation to frequency to be made which demonstrated the influence of nanoparticles on the viscoelastic dampening of the crystal resonance[35]. D/f then infers what changes were made to the viscoelastic properties of the adsorbed layer[35]. Studies have found that by comparing D to f it was possible to determine if the interaction of different molecules with the film adsorbed to the surface of the sensor crystal had single mechanism of interaction or multiple[24,25]. In the case of this study with functionalized nanoparticles diluted in de-ionized water and humic acid there appears to be only one mechanism associated with the interaction of nanoparticles with the SLB. Figure 2.4 shows that the nanoparticles have a fairly linear and horizontal slope for D/f. The data points were very closely packed meaning that there was very little change in both dissipation and frequency despite the 10 min in which the nanoparticles were allotted to interact with the bilayer. The nearly linear and horizontal trend of the slopes seen in Figure 2.4 mean that the nanoparticle interaction with the membrane had very little effect on the viscoelastic properties of the membrane. Given that mass changes were seen in the plots depicting Δf for each of the 5 overtones, it may mean that hydration losses, which were not likely to change the structural integrity of the membrane as losses in mass would have incurred, were much more prevalent. It was likely that lipid was removed at well, but was small enough to not affect the structure of the membrane, in order for water trapped between the membrane and the sensor crystal surface to be released.

2.6.3 Effect of Functionalization on Film Structure

The plots comparing Δf to overtone and dissipation to frequency were able to provide a sense of mass change and how the mass change affected the structure of the membrane. However, it is important to directly compare the viscoelastic changes to the functionalized nanoparticles diluted in de-ionized water and humic acid. Figure 2.5 provided a concise plot comparing D/f values to nanoparticle functionalization for each nanoparticle diluted in both de-ionized water and humic acid in order for direct comparisons to be made. The AuNP functionalized with 2-mercaptoethanol diluted in de-ionized water had a large negative value for D/f indicating that dissipation dominated the value of D/f which means that the viscoelastic changes in the membrane were larger than the mass changes. This was a reasonable response because of the tightly packed data points on the plot of dissipation over frequency. The frequency value was positive for the data of the 2-mercaptoethanol diluted in de-ionized water, meaning that mass was being lost which resulted in conformational changes in the membrane. The remainder of the nanoparticles diluted in de-ionized water and humic acid had positive values for D/f meaning that both dissipation and frequency were positive values and dissipation dominates the ratio. This means that conformational changes in the membrane were fairly significant for small changes in mass for the 12 nm, 1-propanethiol, 2-aminoethanethiol and 3-mercaptopropionic acid AuNPs diluted in de-ionized water and humic acid. It can be seen from Figure 3.5 that the 12 nm, 1-propanethiol, 2-mercaptoethanol and 2-aminoethanethiol AuNPs diluted in de-ionized water and humic acid follow a trend where the nanoparticles diluted in de-ionized water have a slightly smaller D/*f* value than the AuNPs diluted in humic acid. This indicates that in the presence of humic acid, the nanoparticles had a greater effect on conformational changes in the SLB per change in mass. 3-mercaptopropionic acid AuNPs diluted in water have a larger value of D/*f* compared to the same nanoparticles diluted in humic acid which may mean that the humic acid was able to increase electrostatic repulsion for the nanoparticles and reduce the potential toxicity to organisms. However, it was unclear which exact properties of the 3-mercaptopropionic acid the humic acid is able to mitigate to decrease potential toxicity.

2.7 Conclusions

The use of the quartz crystal microbalance with dissipation as a novel technique to test the toxicity of nanoparticles in the presence of natural organic matter (humic acid) with a supported lipid bilayer was successful in determining the mechanisms by which nanoparticles may be toxic. It was possible to determine which physical characteristics of the nanoparticles and by which mechanisms nanoparticles exhibit toxicity and how these parameters would change in the presence of organic matter. The results presented in the study showed that gold nanoparticle toxicity may be associated with the functional groups attached to the nanoparticle surface and that natural organic matter may alter the mechanism and toxicity of the nanoparticles. The 12 nm, 1-propanethiol, 2-mercaptoethanol, 2-aminoethanethiol and 3-mercaptopropionic acid AuNPs diluted in de-ionized water caused positive changes in the frequency which was indicative of mass loss from the adsorbed film (SLB). This may be attributed to losses in lipid and/or hydration in the form of water molecules from the lipid bilayer. The presence of humic acid reduced these losses as much as 75% and stabilized the nanoparticle solution through increasing electrostatic repulsion. The increase of electrostatic forces was known to reduce or eliminate aggregation of nanoparticles in solution[6]. These were significant findings because if gold nanoparticles were released into the environment, they would have reduced effects on organism membranes than if they were introduced in a sterile lab environment.

The experiments done in this study will aid in the development of an assay capable of determining the mechanism of nanoparticle-induced toxicity by separating the molecular effects from the purely physical “nano-specific” effects. Current techniques have proved inadequate and difficult to compare when determining the toxicological effects of nanoparticles because of the diverse properties of nano-materials and the variety of model systems (cells/model membranes) used. Most current studies neglect to separate the role of membrane destabilization from other types of cytotoxic effects. The technology and techniques used in this study will greatly improve the field by using a quantitative approach to study nanoparticle/cell interactions. It will also have the capability of testing a variety of

nano-materials/membrane combinations. The use of AFM techniques in conjunction with the QCM-D would facilitate better understanding of the exact mechanisms by which nanoparticles induce cytotoxicity.

Table 2.1 Properties of 12nm Gold Nanoparticles Used in Humic Acid Studies

Nanoparticle (12 nm)	Functional Group Structure	Polarity	Charge	Zeta Potential (mV)
Bare AuNP		Hydrophilic	Anionic	-36
1-Propanethiol AuNP	$H\text{-}S\text{-}CH_2\text{-}CH_2\text{-}CH_3$	Hydrophobic	Anionic	-51.5
2-Mercaptoethanol AuNP	$H\text{-}S\text{-}CH_2\text{-}CH_2\text{-}OH$	Hydrophilic	Nonionic	-39.8
3-Mercaptoproprionic Acid AuNP	$H\text{-}S\text{-}CH_2\text{-}CH_2\text{-}NH_2$	Hydrophilic	Anionic	-41.5
3-Aminoethanthiol AuNP	$H\text{-}S\text{-}CH_2\text{-}CH_2\text{-}COOH$	Hydrophilic	Cationic	-36.9

*Note: Values and parameters were provided by manufacturer (Nanopartz).

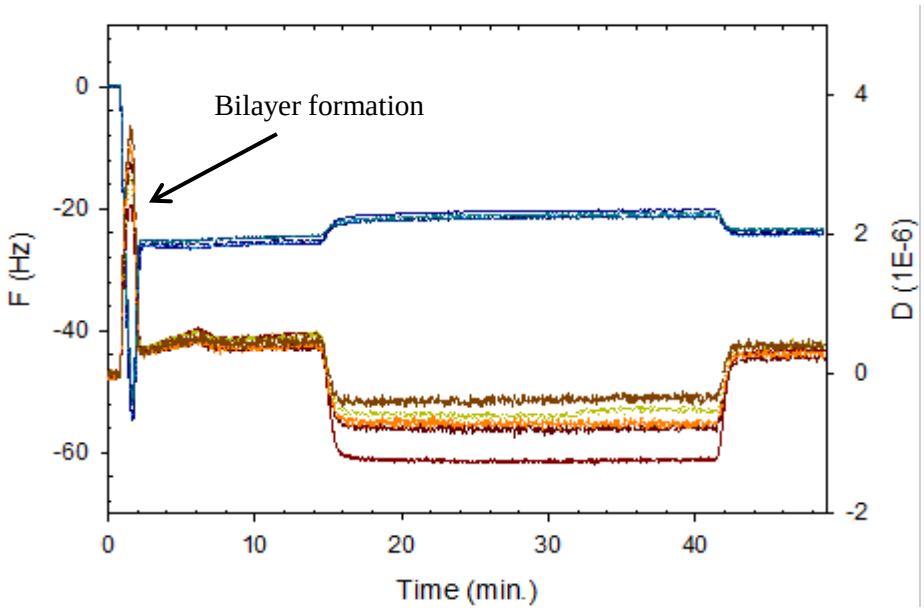

Figure 2.1 Formation of a PC bilayer on SiO_2 crystal. After the bilayer formation, buffer flows through the module to remove un-ruptured or excess vesicles. Water is then introduced to form a viscosity baseline for AuNPs introduced next., followed by another water rinse. Bilayer is rinsed by buffer to complete the experiment. Blue lines represent the frequency for each overtone and red lines represent the dissipation for each overtone. Overtones 3, 5, 7, 9 and 11 are shown on the plot. (Buffer rinse 5:16; water rinse 13:33; NP 21:50; water rinse 32:16; buffer rinse 40:39)

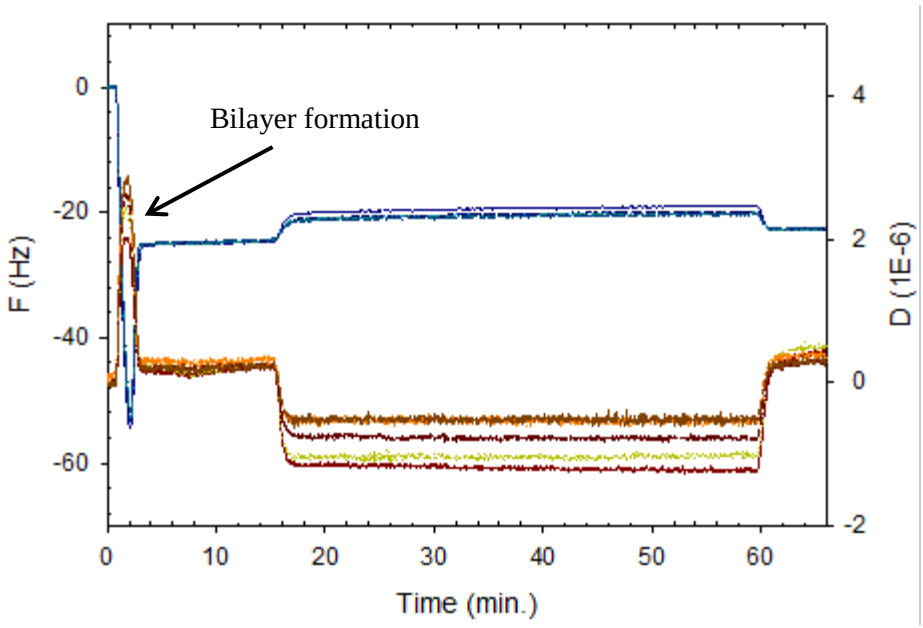

Figure 2.2 Formation of a PC bilayer on SiO_2 crystal. After bilayer formation, buffer flows through the module remove un-ruptured or excess vesicles. Water is introduced followed by the humic acid solution. AuNPs diluted with humic acid are introduced followed by humic acid solution and a water rinse. Buffer is introduced last to complete the experiment. Blue lines represent the frequency fort each overtone and red lines represent dissipation fort each overtone. Overtones 3, 5, 7, 9 and 11 are shown on the plot. (Buffer rinse 6:18; water rinse 14:34; HA solution 22:52; HA+NP 31:10; HA solution 41:27; water rinse 49:42; buffer rinse 58:58)

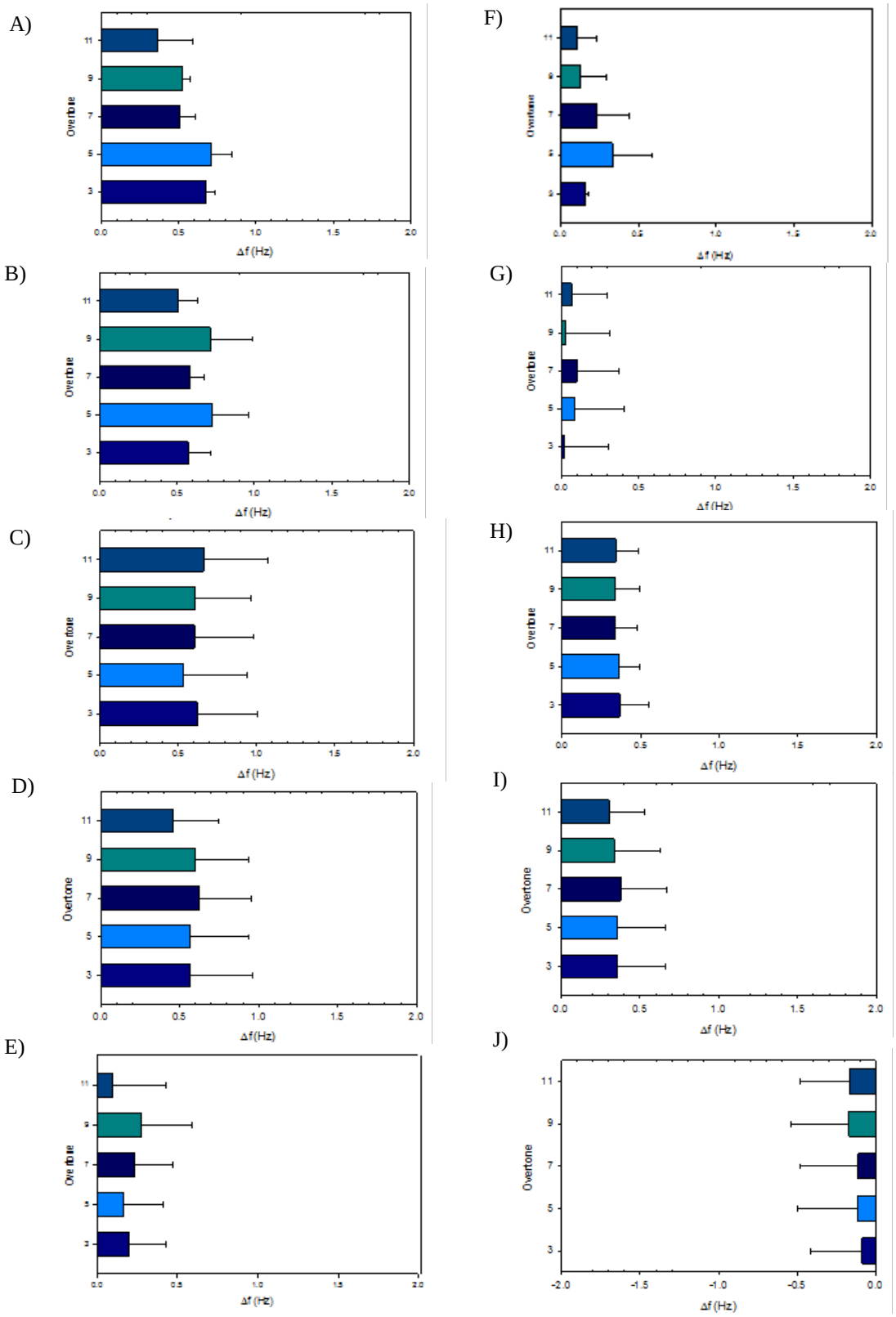

Figure 2.3 Analysis of the frequency change at each overtone for the comparison of AuNPs diluted in de-ionized water and diluted in PMA solution, respectively. Frequency change is a result of nanoparticle introduction and interaction with PC bilayer. A) 12nm AuNP/H_2O, B) 1-propanethiol AuNP/H_2O, C) 2-mercaptoethanol AuNP/H_2O, D) 2-aminoethanethiol AuNP/H_2O, E) 3-mercaptopropionic acid AuNP/H_2O F) 12nm AuNP/HA, G) 1-propanethiol AuNP/HA, H) 2-mercaptoethanol AuNP/HA, I) 2-aminoethanethiol AuNP/HA and J) 2-mercaptoethanol AuNP/HA

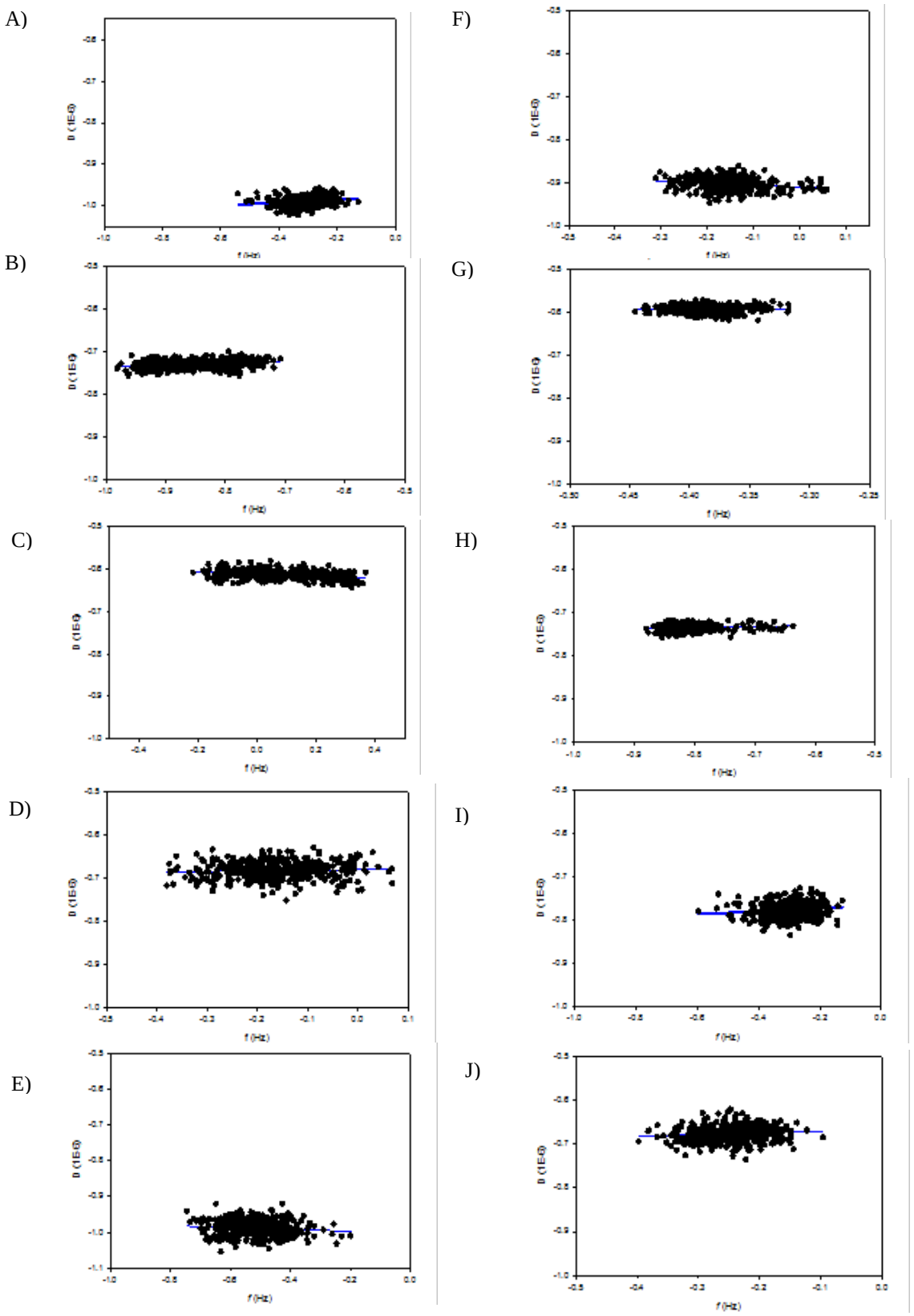

Figure 2.4 Dissipation versus frequency plot at the 7th overtone for AuNPs diluted in PMA interacting with the PC bilayer. The plot illustrates the D/*f* value for nanoparticle introduction over the course of 10min. A) 12nm AuNP/H_2O, B) 1-propanethiol AuNP/H_2O, C) 2-mercaptoethanol AuNP/H_2O, D) 2-aminoethanethiol AuNP/H_2O, E) 3-mercaptopropionic acid AuNP/H_2O F) 12nm AuNP/HA, G) 1-propanethiol AuNP/HA, H) 2-mercaptoethanol AuNP/HA, I) 2-aminoethanethiol AuNP/HA and J) 2-mercaptoethanol AuNP/HA

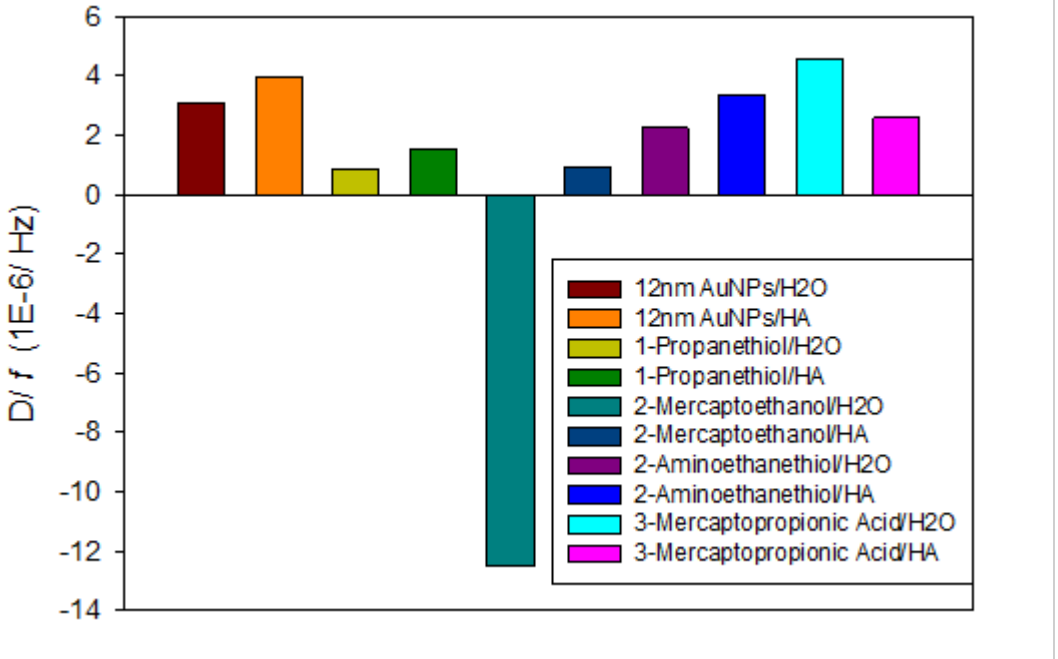

Figure 2.5 Comparison of D/f at the 7th overtone for 12nm AuNP, 1-propanethiol AuNP, 2-mercaptoethanol AuNP, 2-aminoethanethiol AuNP and 3-mercaptopropionic acid AuNP diluted in de-ionized water and humic acid solution. D/f corresponds to membrane rigidity. D/f values were obtained 5 minutes after nanoparticle introduction. Nanoparticles were run for a total of 10 min.

Chapter 2 References

1. Lewinski, N., Colvin, V., Drezek, R. Cytotoxicity of nanoparticles. Small. 2008; 1:26-29.
2. Ghosh, S., Jiang, W., McClements, J.D., Xing, B. Colloidal stability of magnetic iron oxide nanoparticles: Influence of natural organic matter and synthetic polyelectrolytes. Langmuir. 2011; 27:8036-8043.
3. Thomas, C.R., x George, S., Horst, A.M., Ji, Z., Miller, R.J., Peralta-Videa, J.R., Xia, T., Pokhrel,S., Mädler, L., Gardea-Torresdey, J.L., Holden, P.A., Keller, A.A., Lenihan, H.S., Andre E. Nel, A.E., Zink, J.I. Nanomaterials in the environment: From materials to high-throughput screening to organisms. ACS nano; 2011:5:1:13-20.
4. Domingos, R.F., Tufenkji, N., Wilkinson, K.J. Aggregation of titanium dioxide nanoparticles: Role of fulvic acid. Environ. Sci. and Tech. 2009; 43:1282-1286.
5. Gao, J., Powers, K., Wang, Y., Zhou, H., Roberts, S.M., Moudgil, B.M., Koopman, B., Barber, D.S. Influence of suwannee river humic acid on particle properties and toxicity of silver nanoparticles. Chemosphere. 2012; 89:96-101.
6. Hu, X., Chen, Q., Jiang, L., Yu, Z., Jiang, D., Yin, D. Combined effects of titanium dioxide and humic acid on the bioaccumulation of cadmium in zebrafish. Environ. Pollution. 2011; 159:1151-1158.
7. Mileyeva-Biebesheimer, O.N., Zaky, A., Gruden, C.L. Assessing the impact of titanium dioxide and zinc oxide nanoparticles on bacteria using a fluorescent-based cell membrane integrity assay. Environ. Engineer. Sci. 2010; 27:4:329-335.
8. Fabrega, J., Luoma, S.N., Tyler, C.R., Galloway, T.S., Lead, J.R. Silver nanoparticles: Behaviour and effects in aquatic environment. 2011; 37:517-531.
9. Jo, H.J., Choi, J.W., Lee, S.H., Hong, S.W. Acute toxicity of Ag and CuO nanoparticles suspensions against Daphnia magna: The importance of their dissolved fraction varying with preparation methods. J. Hazardous Materials. 2012; 227-228:301-308.
10. Rico, C.M., Majunmdar, S., Duarte-Gardea, M., Peralta-Videa, J.R., Gardea-Torresday, J.L. Interaction of nanoparticles with edible plants and their possible implications in the food chain. J. Agricultural and Food Chemistry. 2011; 59:3485-3498.
11. Chen, K.L., Elimelech, M. Influence of humic acid on the aggregation kinetics of fullerene (C_{60}) nanoparticles in monovalent and divalent electrolyte solutions. J. Colloid and Interface Sci. 2007;309:126-134.
12. Diegoli, S., Manciulea, A.L., Begum, S., Jones, I.P., Lead, J.R., Preece, J.A. Interaction between manufactured gold nanoparticles and naturally occurring organic molecules. Sci. Total Environ. 2008;402:51-61.
13. Li, M., Huang, C.P. Stability of oxidized single-walled carbon nanotubes in the presence of simple electrolytes and humic acid. Carbon. 2010; 48:4527-4534.
14. Lin, D., Ji, J., Long, Z., Yang, K., Wu, F. The influence of dissolved and surface-bound humic acid on the toxicity of TiO_2 nanoparticles to Chlorella sp. Water Research. 2012; 46: 4477-4487.

15. Schulz, M., Olubummo, A., Binder, W.H. Beyond the lipid-bilayer: interaction of polymer and nanoparticles with membranes. Soft Matter. 2012; 8:4849-4864.
16. Monteiro-Riviere, N.A., Inman, A.O., Zhang, L.W. Limitations and relative utility of screening assays to assess engineered nanoparticle toxicity in a human cell line. Toxicology and Applied Pharmacology. 2009; 234:222-235.
17. Luo, J., Chan, W.B., Wang, L., Zhong, C.J. Probing interfacial interactions of bacteria on metal nanoparticles and substrates with different surface properties. Int. J. Antimicrobial Agents. 2010; 36:529-556.
18. Ginzburg, V.V., Balijepalli, S. Modeling of thermodynamics of the interaction of nanoparticles with cell membranes. Nano Letters. 2007; 7:12:3716-3722.
19. Hou, W.C., Moghadam, B.Y., Corredor, C., Westerhoff, P., Posner, J.D. Distribution of functionalized gold nanoparticles between water and lipid bilayers as model cell membranes. Environ. Sci. and Tech. 2012; 46:1869-1876.
20. Keller, C.A., Glasmastar, K., Zhdanov, V.P., Kasemo, B. Formation of supported membranes from vesicles. Physical Review Letters. 2000; 84:23:5443-5446.
21. Mechler, A., Praporski, S., Atmuri, K., Boland, M., Separovic, F., Martin, L.L. Specific and selective peptide-membrane interactions revealed using quartz crystal microbalance. Biophysical Journal. 2007; 93:3907-3916.
22. Bothun, G. Hydrophobic silver nanoparticles trapped in lipid bilayers: Size distribution, bilayer phase behavior and optical properties. J Nanobiotech. 2008; 6:13.
23. Park, S.H., Oh, S.G., Mun, J.Y., Han, S.S. Loading of gold nanoparticles inside the DPPC bilayers of liposome and their effects on membrane fluidities. Colloids and Surfaces B: Biointerfaces. 2006; 48:112-118.
24. Feiler, A.A., Sahlholm, A., Sandberg, T., Caldwell, K.D. Adsorption and viscoelastic properties of fractionated mucin (BSM) and bovine serum albumin (BSA) studied with quartz crystal microbalance (QCM-D). J. Colloid and Interface Sci. 2007; 315:475-481.
25. Hook, F., Ray, A., Norden, B., Kasemo, B. Characterization of PNA and DNA immobilization and subsequent hybridization with DNA using acoustic-shear-wave attenuation measurements. Langmuir. 2001; 17:8305-8312.

Concluding Remarks

The quartz crystal microbalance with dissipation (QCM-D) was used as a novel system in order to obtain quantitative results reflecting the interaction of gold nanoparticles with a supported lipid bilayer. The acoustic techniques employed by the QCM-D were able to detect changes in mass and structure of the thin lipid bilayer (5 nm diameter) adsorbed to the surface of the sensor crystal in real time, through measurements of frequency and dissipation. The shifts in resonance frequency of the piezoelectric quartz sensor crystal were related to the amount of mass adsorbed/desorbed to/from the crystal surface. Dissipation shifts were related to changes in the viscoelastic properties of the supported lipid bilayer, where soft, flexible films resulted in larger responses. Results detected were found to be a function of nanoparticle or nanoparticle/NOM complex interactions with the supported bilayer and not a function of changes in viscosity of bilayer interaction with NOM.

It was important to first characterize the size effects of nanoparticle interaction with a lipid bilayer in order to establish a baseline for further studies done in the presence of natural organic matter. The results showed that size only minimally impacted the difference in interactions seen for the gold nanoparticles $\geq$ 5 nm diluted in water. The 2 nm AuNPs diluted in water were deemed to have no interaction, whereas the larger sized particles used in the study removed mass from the adsorbed film. Dilution in PMA was seen to significantly impact the 2 and 5 nm AuNPs, providing the means for solubilization into the lipid bilayer by presumably modifying the NP surface through interaction of PMA with stabilizing groups present on the NP surface, creating a hydrophobic coating. It has been shown in several studies that hydrophobicity plays a key role in nanoparticle penetration of lipid bilayers[1,2]. It was generally found that nanoparticle interaction with the bilayer had nominal effects of the viscoelastic properties of the bilayer, although 2 nm AuNP/PMA complexes showed a unique trend with possibly two kinetically different reactions during membrane penetration which could possibly be attributed to lipid or

nanoparticle rearrangement within the bilayer. The 10 and 40 nm AuNP in the presence of PMA showed slight changes the amount of mass removed compared to particles diluted in de-ionized water.

In order to provide substantially significant results in regards to environmental conditions it was important to use a complex class of naturally occurring organics, such as humic acid, which has been studied and characterized thoroughly. Functionalized gold nanoparticles were used in order to mimic the complex functionality found on particles released into the environment. The results presented showed that toxicity of the nanoparticles may be linked to functionality and the presence of humic acid. It is known that the aggregation of gold nanoparticles coupled with their unique surface properties may cause cytotoxic effects and aggregation is key component[3]. It has been shown in many studies that the presence of humic acid may stabilize the system through electrostatic repulsion and mitigate aggregation[4-8]. In our study it was found that humic acid was able to reduce mass losses to the supported lipid bilayer by up to 75% by coating the nanoparticles. Functionalized gold nanoparticles diluted in water caused mass reduction from the adsorbed film attributed to lipid loss the bilayer surface which produced a more rigid film associated with strain inflicted by lipid chain stretching to fill voids.

Overall, the QCM-D was found to provide valuable information regarding the possible toxic properties and mechanisms in which different gold nanoparticle interact with a supported lipid bilayer under environmental conditions. The information provided by the studies performed has shed much light on the interaction of gold nanoparticles with a supported lipid bilayer in the presence of model natural organic matter. The results from studies done with humic acid verified the work of other studies that similarly concluded toxicity may be moderated or eliminated by reducing the aggregation of nanoparticles through humic acid adsorption to the NP surface, increasing the electrostatic repulsion of the particles.

The experiments done in this study are the first steps towards developing an assay capable of mechanism determination of nanoparticle-induced cytotoxicity by decoupling molecular effects from “nano-specific” effects. Current techniques employed have been inadequate because of their inability to separate the role of membrane destabilization from other types of cytotoxic effects. Consequently, the variety of model cells, nanoparticle preparations and systems used to determine toxicity has made it

impossible to distinguish which physicochemical properties are responsible for toxicity. The technology and techniques used in this study will greatly improve the field by solidifying one technique to use in the quantitative approach studying nanoparticle/cell interactions. It will also have the capability of testing a variety of nano-materials/membrane combinations. The use of AFM techniques in conjunction with the QCM-D would be highly beneficial by facilitating better understanding of the exact mechanisms by which nanoparticles induce cytotoxicity.

References

1. Bothun, G. Hydrophobic silver nanoparticles trapped in lipid bilayers: Size distribution, bilayer phase behavior and optical properties. J Nanobiotech. 2008; 6:13.
2. Park, S.H., Oh, S.G., Mun, J.Y., Han, S.S. Loading of gold nanoparticles inside the DPPC bilayers of liposome and their effects on membrane fluidities. Colloids and Surfaces B: Biointerfaces. 2006; 48:112-118.
3. Cui, W., Li, J., Zhang, Y., Rong, H., Lu, W., Jiang, L. Effects of aggregation and surface properties of gold nanoparticles on cytotoxicity and cell growth. Nanomedicine: Nanotech., Biology and Medicine. 2012; 8:46-53.
4. Diegoli, S., Manciulea, A.L., Begum, S., Jones, I.P., Lead, J.R., Preece, J.A. Interaction between manufactured gold nanoparticles and naturally occurring organic molecules. Sci. Total Environ. 2008;402:51-61.
5. Gao, J., Powers, K., Wang, Y., Zhou, H., Roberts, S.M., Moudgil, B.M., Koopman, B., Barber, D.S. Influence of suwannee river humic acid on particle properties and toxicity of silver nanoparticles. Chemosphere. 2012; 89:96-101.
6. Chen, K.L., Elimelech, M. Influence of humic acid on the aggregation kinetics of fullerene (C_{60}) nanoparticles in monovalent and divalent electrolyte solutions. J. Colloid and Interface Sci. 2007;309:126-134.
7. Li, M., Huang, C.P. Stability of oxidized single-walled carbon nanotubes in the presence of simple electrolytes and humic acid. Carbon. 2010; 48:4527-4534.
8. Lin, D., Ji, J., Long, Z., Yang, K., Wu, F. The influence of dissolved and surface-bound humic acid on the toxicity of TiO_2 nanoparticles to Chlorella sp. Water Research. 2012; 46: 4477-4487.